

Article

Not peer-reviewed version

Net Zero Agrivoltaic Arrays for Agrotunnel Vertical Growing Systems: Energy Analysis and System Sizing

[Nima Asgari](#) , [Uzair Jamil](#) , [Joshua M. Pearce](#) *

Posted Date: 26 June 2024

doi: [10.20944/preprints202406.1820.v1](https://doi.org/10.20944/preprints202406.1820.v1)

Keywords: aeroponics; agrivoltaics; agrotunnel; hydroponics; photovoltaic; solar energy; vertical farming



Preprints.org is a free multidiscipline platform providing preprint service that is dedicated to making early versions of research outputs permanently available and citable. Preprints posted at Preprints.org appear in Web of Science, Crossref, Google Scholar, Scilit, Europe PMC.

Copyright: This is an open access article distributed under the Creative Commons Attribution License which permits unrestricted use, distribution, and reproduction in any medium, provided the original work is properly cited.

Article

Net Zero Agrivoltaic Arrays for Agrotunnel Vertical Growing Systems: Energy Analysis and System Sizing

Nima Asgari ¹, Uzair Jamil ² and Joshua M. Pearce ^{2,*}

¹ Department of Electrical & Computer Engineering, Western University, London, ON, Canada; nasgari@uwo.ca; ujamil@uwo.ca

² Ivey School of Business, Western University, London, ON, Canada

* Correspondence: joshua.pearce@uwo.ca

Abstract: To control the volatility and reduce the electricity costs for indoor farming, the agrivoltaics agrotunnel introduced here uses: 1) high insulation for a building dedicated to vertical growing, 2) high-efficiency LED lighting, 3) heat pumps (HPs), and 4), solar photovoltaics (PV) provide known electric costs for 25 years. In order to size the PV array, this study develops a thermal model for agrotunnel load calculations and validates it using the Hourly Analysis Program and measured data so the effect of plants' evapotranspiration can be included. HPs are sized, plug loads (i.e., water pump energy needed to provide for the hybrid aeroponics/hydroponics system, DC power running the LEDs hung on grow walls, and dehumidifier assisting in moisture condensation in summer) are measured/modeled. Ultimately, all models are combined to establish an annual load profile for an agrotunnel that is then used to model the necessary PV to power the system throughout the year. The results find that agrivoltaics to power an agrotunnel range from 40 to 50kW and make up an areas from 3.2 to 10.48 m²/m² of an agrotunnel footprint. Net zero agrotunnels are technically viable although future work is needed to deeply explore the economics of localized vertical food growing systems.

Keywords: aeroponics; agrivoltaics; agrotunnel; hydroponics; photovoltaic; solar energy; vertical farming

1. Introduction

Agriculture has enormous negative impacts on the natural environment (22% of 2019 global greenhouse gas emissions) [1], but indoor growing can significantly reduce the environmental impact of agriculture, especially by minimizing transportation emissions [2,3]. Moreover, indoor growing can drastically reduce water usage compared to traditional farming methods [4]. Indoor farming also allows increased crop productivity per unit area and reduces the time required to reach plant maturity [4]. Indoor growing can reduce and in some cases eliminate the use of harmful herbicides or pesticides promoting healthier produce [5]. Unlike traditional outdoor farming, indoor growing enables year-round production, ensuring a consistent food supply regardless of seasonal changes or weather conditions [6,7]. The technology also provides spatial efficiency and land use optimization [7]. With advancements in LED lighting technology and optimized envelope, indoor growing operations can minimize energy consumption, mitigating their carbon footprint [8,9]. Closed-loop systems in indoor growing can minimize waste production by recycling water, nutrients, and organic matter, contributing to a circular economy model [10,11]. Indoor growing also helps preserve biodiversity by allowing for more diverse and resilient ecosystems in agricultural regions [12]. Unfortunately, indoor growing in general has a major problem: increased energy costs have forced many indoor growing operations into bankruptcy [3], which hits vertical growers particularly hard [13]. High energy costs and energy price volatility have made even startups with hundreds of millions of dollars of funding go bankrupt [14].

To overcome electrical costs for indoor farming, the agrivoltaics agrotunnel introduced here uses four approaches: 1) high insulation for a building dedicated to vertical growing, 2) high efficiency light emitting diodes (LEDs) for lighting, 3) the use of heat pumps (HPs), and 4) to control the volatility and reduce the electricity costs, solar photovoltaics (PV) provide for a known LCOE and a 25-year lifetime. All these approaches have been combined in an agrivoltaics agrotunnel where agrivoltaics arrays on the outside provide power for the grow lights and water pumps and other electrical equipment on the inside. The core concept involves either an earth and vegetation-covered tunnel (Figure 1a) or a mobile unit (Figure 1b) housing high-density vertical aeroponic-hydroponic hybrid systems illuminated by high-efficiency LED grow lights. Next to the agrotunnel fixed/variable tilt agrivoltaics PV arrays [15] are shown, which provide all of the power necessary to operate the agrotunnel.

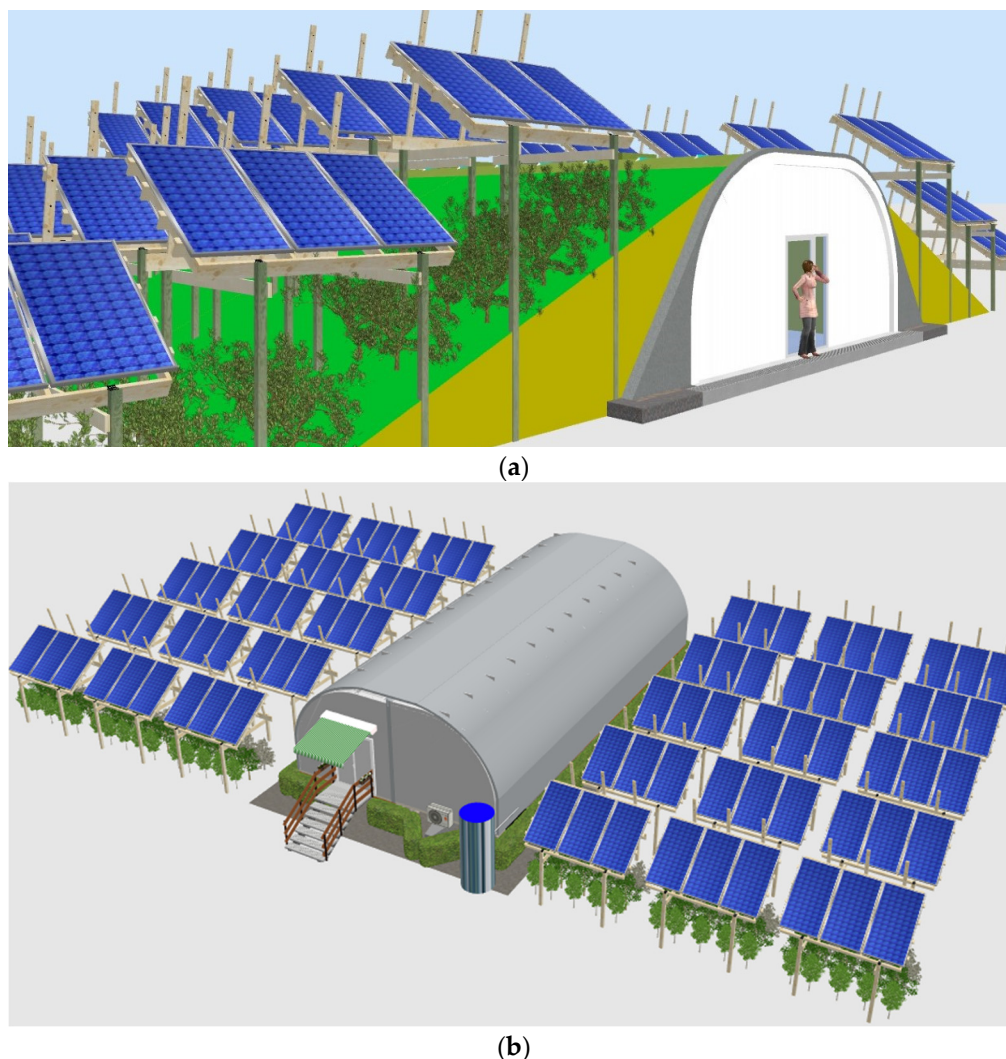


Figure 1. Agrivoltaic agrotunnel: (a) subterranean agrivoltaic agrotunnel; (b) semi-mobile agrivoltaic agrotunnel.

PV technology has declined in price for decades [16,17], making it the lowest-cost electricity generation technology [18,19]. This provides an opportunity to control the costs of indoor growing. Already because of this cost advantage, PV is the most rapidly-expanding electricity source [20,21] and dominates new sources of power [22]. With the growth of PV, which demands large surface areas to provide large amounts of energy there have been land-use conflict associated with installing PV plants on farmland [23–26]. Fortunately, this can be rectified with agrivoltaics, which refers to the dual use of land for clean electricity generation with PV and agriculture [27–31]. This increases land efficiency [32,33] and agrivoltaic systems have proven to be economically viable as they provide

farmers with dual stream of revenue – one through generation of electricity and one through the produce/crop yield [30,34–38]. To push this concept further this paper investigates the potential of using agrivoltaics to power the even more land use efficient indoor growing inside an agrotunnel.

In order to size the net-zero agrivoltaics array that is necessary to support an agrotunnel, this study first develops a thermal model for load calculations in agrotunnel, which has been validated using the results of a commercial building's load calculation with the Hourly Analysis Program (HAP). Using measured data, the effect of plants' evapotranspiration is included subsequently as it is not incorporated in HAP software. The size of heat pumps (HPs) needed to maintain a constant temperature in the agrotunnel is determined in the next step. Next, plug loads (i.e., water pump energy needed to provide for the hybrid aeroponics/hydroponics system, DC power running the LEDs hung on the grow walls, and dehumidifier assisting in moisture condensation in summer) are measured/modeled. Ultimately, all models are combined to establish an annual load profile for an agrotunnel (also verified based on two month performance) that is then used to model the necessary PV to power the system throughout the year. The results are discussed, and future work is outlined to completely solarize agrivoltaics agrotunnels.

2. Agrivoltaic Agrotunnel

The agrotunnel (Food Security Structures Canada (FSSC) [39], London, ON) presents a solution to combat food insecurity by offering an easily assembled, scalable, and sustainable indoor vertical farming structure. It is designed to withstand extreme climate conditions and can be adapted to various locations. FSSC uses fiber reinforced polymer (FRP) construction to enhance portability, strength, and lightweight design to reduce the embodied energy and emissions for transportation. This innovative growing chamber enables precise control of light, humidity, and temperature, facilitating year-round cultivation of hybrid-aeroponic fruits and vegetables in harsh environments. Assembling the 1.2 m × 2.4 m panels allows for easy transportation of components. The detailed dimensions and thermal resistances of the agrotunnel envelope are illustrated in Figure 2.

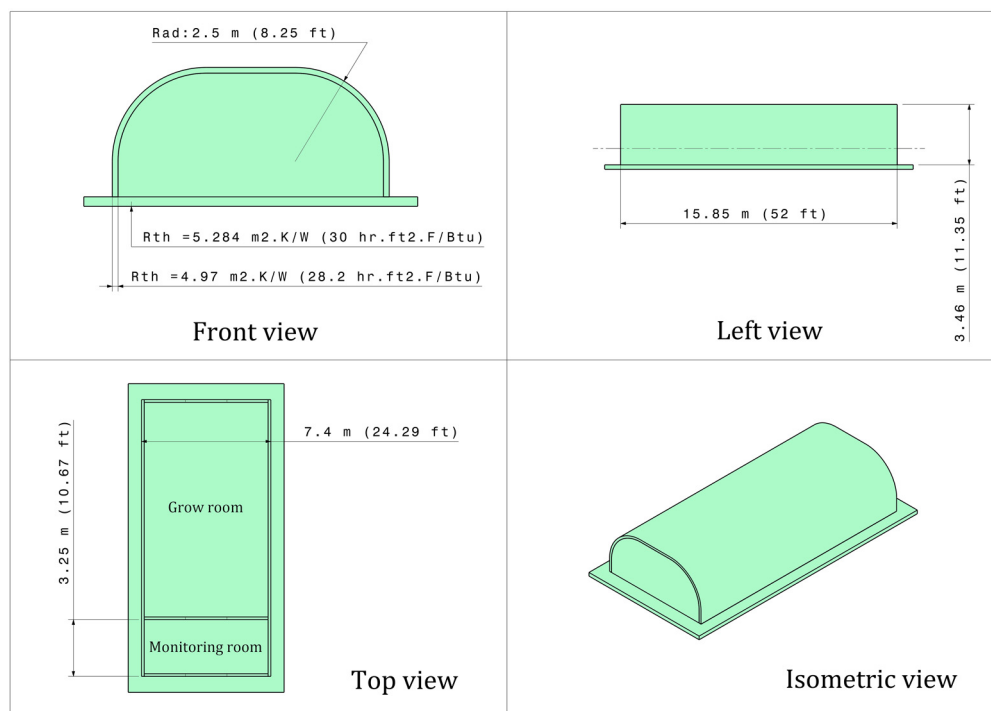


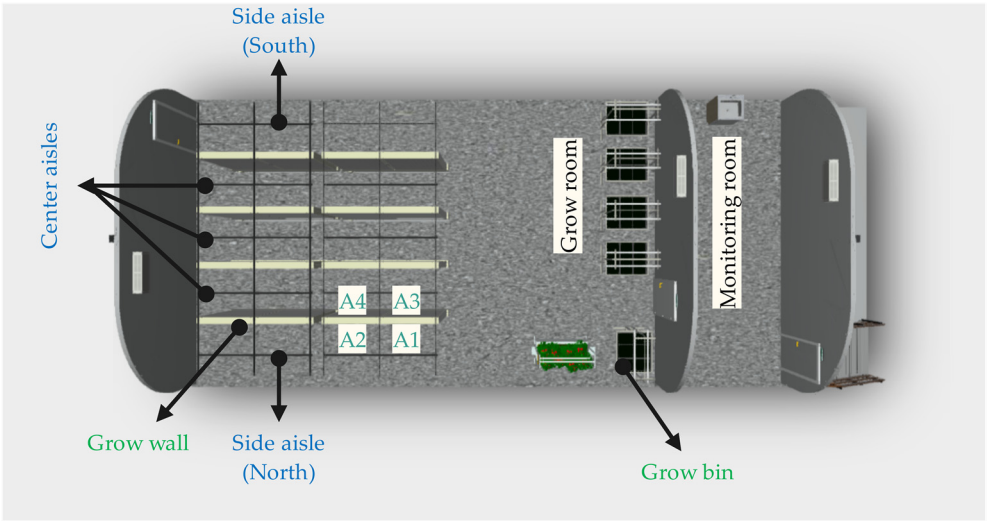
Figure 2. The CAD model including the dimensions and the thermal resistances of the envelope.

The agrotunnel under study is located at the Western Innovation for Renewable Energy Deployment (WIRED) in London, Ontario (Figure 3a). As shown in Figure 3b, the design is composed of two sections (grow room and monitoring room). 8 grow walls, each with two sides and two mini

walls for each side are installed in the growing room in addition to 6 grow bins. Utilizing the same growing technology as the grow walls featuring adjustable lighting brackets, the grow bins offer an ideal growing setting for root vegetables and other plants that demand greater space.



(a)



(b)

Figure 3. The Agrotunnel under study: (a) actual structure established at WIRED; (b) Detailed model (Top view).

All the growing facilities are fed by low wattage and low voltage LED lights produced by Better Grow Lights [40]. These commercial lights are specifically designed for high density plant spacing and come with three 180 ° (BGL180A), 180 ° (BGL180C), and 360 ° (BGL360A) designs. BGL180A lights are hung on the side aisles as well as top of the grow bins, and BGL360A are hung on the center aisles, as shown in Figure 4. BGL180C are horizontally hung on top of the grow bins. In the agrotunnel, there are 28 BGL180A each with 75 W, 42 BGL360A each with 100 W, and 12 BGL180C each with 30 W wattage (11 in grow room and 1 in monitoring room).



Figure 4. The location of lights and their applications inside the agrotunnel: (a) BGL180A on the side aisles; (b) BGL360A on the center aisles; (c) BGL180C on the grow bin.

3. Methodology

The agrotunnel's load is made up of four sub systems: lights, water pumps, heat pump (HP), and a dehumidifier. A dehumidifier is operated to assist HPs in maintaining the relative humidity (RH) at a desired level. The HP is the major component in meeting the thermal (sensitive and latent)

loads of the system. Artificial lighting also has a major contribution to increasing the temperature of the agrotunnel's microclimate. All these loads are characterized as shown in Figure 5. Sizing all the thermal and electrical equipment would be done based on the loads as the results of the structure's specifications and the circumstances the plants will grow under.

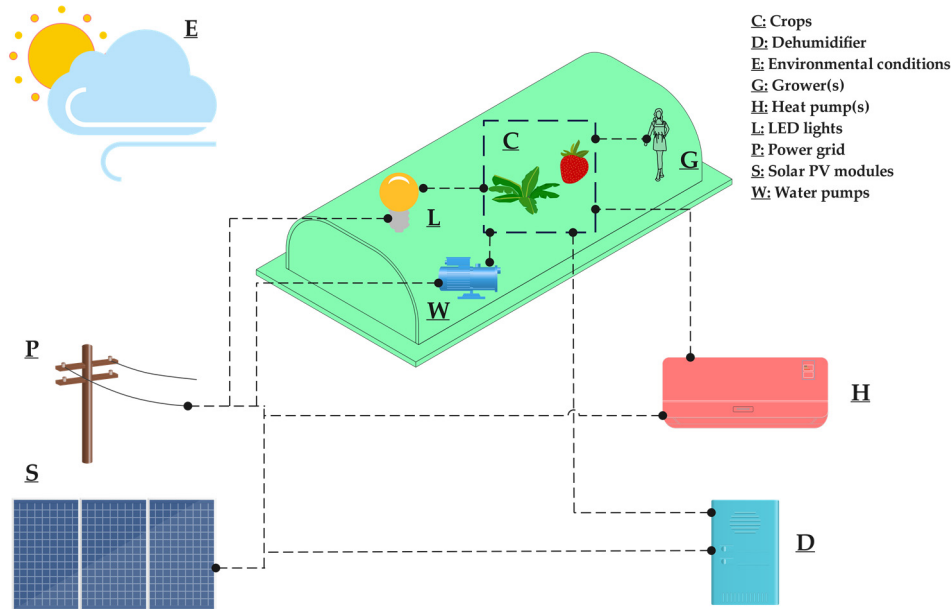


Figure 5. Schematic of the agrotunnel integrated with the energy provision equipment.

3.1. Thermal Model

The load calculations of the agrotunnel are estimated using the following thermal model developed. It is assumed that all the lights are on and planted crops are mature enough. Meanwhile, one person is doing some non-strenuous work such as planting, harvesting, watering, etc. in the building. The following sub-models are developed based on the load calculation principles [41].

3.1.1. External Loads

CLTD/CLF method, described in the 1997 AHSRAE Fundamentals [42], is used to calculate the transmission load of the agrotunnel, which is the most practical method for sizing the HVAC equipment while being simple.

Equation (1) is used for calculating the heat gains through the walls, the roof, and the floor. Cooling load temperature difference (CLTD) considers the collective impact of variations in indoor and outdoor temperatures, daily temperature fluctuations, solar radiation, and heat retention within the building structure. The values are determined using the tables provided in Chapter 28th of ASHRAE Fundamentals Handbook [42].

$$\dot{Q}_{cc} = \sum \frac{A_k}{R_{tot,k}} CLTD + \frac{A_{floor}}{R_{tot,floor}} (T_o - T_i), \quad (1)$$

where, \dot{Q}_{cc} represents the heat losses due to the conduction and convection transmission through the envelope. A_k is the surface area of each part of the envelope (m^2 or ft^2) except for the floor and A_{floor} stands for the surface area of the floor. $R_{tot,k}$ corresponds to the conduction and convection thermal resistance of each part of the envelope ($m^2.K/W$ or $hr. ft^2.F/Btu$), which can be calculated by Equation (2) [43]:

$$R_{tot,k} = R_{conv,o} + R_{cond} + R_{conv,i}, \quad (2)$$

T_i and T_o are the indoor design temperature and the outdoor temperature ($^{\circ}C$ or $^{\circ}F$), respectively. As the ASHRAE tables offer hourly CLTD values based on a standard scenario, such as an outdoor

maximum temperature of 95 °F, mean temperature of 85 °F, and a daily temperature range of 21 °F, Equation (1) is modified through Equations (3-5) to accommodate correction factors for situations deviating from this base case. CLTD values of the base case for the material used in the envelope are tabulated in Table 1.

$$\dot{Q}_{cc} = \sum \frac{A_k}{R_{tot,k}} CLTD_{corrected} + \frac{A_{floor}}{R_{tot,floor}} (T_o - T_i), \quad (3)$$

$$CLTD_{corrected} = CLTD + (78 - T_i) + (T_{o,mean} - 85), \quad (4)$$

$$T_{o,mean} = T_{o,max} - \frac{DRT}{2}, \quad (5)$$

the daily range of temperature (DRT) indicates the difference between the maximum and the minimum temperature within 24 hours. For the floor transmission, $(T_o - T_i)$ will be simply used.

Table 1. CLTD values of the base case for the material used in the agrotunnel's envelope *.

Hour	Roof	North	South	East	West
1	37	17	21	20	35
2	32	15	18	17	30
3	27	13	15	14	25
4	23	11	12	12	21
5	19	9	10	10	17
6	15	7	8	8	14
7	12	5	6	6	11
8	10	4	5	5	8
9	9	4	4	7	7
10	10	4	3	12	6
11	12	5	4	19	6
12	17	7	6	26	7
13	23	8	10	32	8
14	30	10	14	36	10
15	37	12	20	37	12
16	44	15	25	37	16
17	50	17	29	37	22
18	55	19	33	36	30
19	57	21	34	34	37
20	58	22	34	33	44
21	56	23	32	31	48
22	52	23	30	29	48
23	47	22	27	26	45
24	42	20	24	23	41

* The values must be used in calculations in IP units.

The sensible and latent loads caused by infiltration can be calculated using Equations (6) & (7), respectively.

$$\dot{Q}_{sens,inf} = n_{ACH} V_{AT} \rho_a c_{p_a} (T_o - T_i), \quad (6)$$

$$\dot{Q}_{lat,inf} = n_{ACH} V_{AT} \rho_a (\omega_o - \omega_i) h_{fg}, \tag{7}$$

here, V_{AT} is the total volume of the agrotunnel (m^3 or ft^3). ρ_a and Cp_a are the air density (kg/m^3 or lb_m/ft^3) and specific heat capacity ($\text{kJ}/\text{kg}\cdot\text{K}$ or $\text{Btu}/\text{lb}_m\cdot\text{F}$), respectively. n_{ACH} indicates the infiltration rate in ACH (hr^{-1}), which usually is 0.25 for a newly constructed and well-insulated building [44]; for this specific building without any windows and completely sealed walls, however, 0.1 will be a rational assumption. Also, ω_i and ω_o denote the indoor and outdoor humidity ratio in ($\text{kg}_w/\text{kg}_{da}$ or $\text{lb}_{m,w}/\text{lb}_{m,da}$), respectively, and h_{fg} corresponds to the enthalpy of vaporization of water in (kJ/kg or Btu/lb_m).

3.1.2. Lights

The waste heat dissipated by the LED lights mainly depends on their power and the cooling load factor ($F_{CLF,light}$), which can vary within a day based on the operating schedule of lights. $F_{CLF,light}$ would be 1 for the case lights are on for 24 hours. Otherwise, Table 2 will be used for one story building [42].

Table 2. Cooling Load Factor (CLF) for lights [42].

Number of hours after lights turned on	Hours lights on				
	8	10	12	14	16
1	0.72	0.73	0.74	0.75	0.77
2	0.8	0.81	0.82	0.84	0.85
3	0.84	0.85	0.86	0.87	0.89
4	0.87	0.87	0.88	0.89	0.91
5	0.88	0.89	0.9	0.91	0.92
6	0.89	0.9	0.91	0.92	0.93
7	0.9	0.91	0.92	0.92	0.93
8	0.91	0.92	0.92	0.93	0.94
9	0.23	0.92	0.93	0.94	0.95
10	0.15	0.93	0.94	0.94	0.95
11	0.11	0.25	0.94	0.95	0.95
12	0.09	0.16	0.95	0.95	0.96
13	0.08	0.13	0.26	0.96	0.96
14	0.07	0.11	0.18	0.96	0.97
15	0.07	0.09	0.14	0.27	0.97
16	0.06	0.08	0.12	0.19	0.97
17	0.05	0.08	0.1	0.15	0.28
18	0.05	0.07	0.09	0.13	0.2
19	0.05	0.06	0.08	0.11	0.16
20	0.04	0.06	0.08	0.1	0.13
21	0.04	0.05	0.07	0.09	0.12
22	0.03	0.05	0.06	0.08	0.11
23	0.03	0.04	0.06	0.08	0.1
24	0.03	0.04	0.05	0.07	0.09

* The values must be used in calculations in IP units.

Equation (8) gives the waste heat dissipated by lights in (W or Btu/hr). n_{lights} , P_{lights} , F_{lu} , and F_a are the number of lights used, the power of lights used in (W), the lights use factor, which can be assumed to be 1, and the ballast allowance factor, which can be assumed 1 for LED lights [45].

$$\dot{Q}_{lights} = n_{lights}P_{lights}F_{lu}F_aF_{CLF,light},$$

(8)

3.1.3. People

Each person working in agrotunnel brings in both sensible and latent loads. Sensible and latent heat gained by a person who is doing sedentary (standing or walking slowly) or some light works are 92.4 W (315 Btu/hr) and 95.3 W (325 Btu/hr), respectively [42]. Total cooling load caused by the presence of the people in agrotunnel can be calculated using Equation (9):

$$\dot{Q}_{people} = \dot{Q}_{sens,people} + \dot{Q}_{lat,people} = n_{people} \times (315 \times F_{CLF,people} + 325 \times F_{CLF,lat,people}),$$

(9)

where, n_{people} represents the total number of people who are working in agrotunnel, and $F_{CLF,people}$ stands for the cooling load factor of people, based on the number of hours they work each day. In the basic scenario in the present study, it is assumed that one person is working 8 hours 7 days of week from 9 AM to 5 PM. Therefore, using Table 3, the $F_{CLF,people}$ will be extracted. $F_{CLF,lat,people}$ includes either 0 or 1 to consider the effect of the grower’s presence.

Table 3. Cooling Load Factor (CLF) for people [42].

Number of hours after entry into the space	Hours in space			
	4	6	8	10
1	0.59	0.6	0.61	0.62
2	0.67	0.67	0.68	0.69
3	0.13	0.72	0.73	0.74
4	0.09	0.76	0.77	0.77
5	0.08	0.2	0.8	0.8
6	0.06	0.16	0.83	0.83
7	0.05	0.13	0.26	0.85
8	0.05	0.11	0.2	0.87
9	0.04	0.1	0.17	0.3
10	0.04	0.08	0.15	0.24
11	0.03	0.07	0.13	0.2
12	0.03	0.06	0.11	0.17
13	0.02	0.05	0.09	0.15
14	0.02	0.05	0.08	0.13
15	0.02	0.04	0.07	0.11
16	0.01	0.03	0.06	0.1
17	0.01	0.03	0.05	0.08
18	0.01	0.03	0.05	0.07
19	0.01	0.02	0.04	0.06
20	0.01	0.02	0.03	0.05
21	0.01	0.02	0.03	0.05
22	0.01	0.01	0.03	0.04
23	0.01	0.01	0.02	0.04

24 0 0.01 0.02 0.03

* The values must be used in calculations in IP units.

3.1.4. Evapotranspiration of Plants

There are many models of evapotranspiration [46,47], which incorporate the effect of various parameters, interpretation of which is beyond the scope of this study. In this case 8 walls each with 720 pots for a total of 5,760 all of which are being watered aeroponically at potentially different stages of growth and different species present an enormously complicated system. A more straightforward way to estimate the evapotranspiration load in a grow room involves calculating the net water consumption of plants. This entails measuring the volume of irrigation water introduced into the agrotunnel and subtracting the volume of water drained away [48]. The average amount of water consumed (\dot{m}_{water}) can be estimated in (kg/s or lb_m/hr). Hence, the heat of vaporization will be calculated using Equation (10):

$$\dot{Q}_{evap} = \dot{m}_{water} h_{fg} \quad (10)$$

During this process, the moist soil and plants' leaves absorb heat from the environment, causing a temperature drop (sensible heating load), then evaporate. The energy absorbed is converted to latent heat of vapor in the air, which causes an increase in the humidity level of the microclimate (the latent cooling load). This transfer in energy leads to a constant enthalpy process, which is shown in Figure 6. Since the evapotranspiration of mature plants in a fully planted agrotunnel can be significant, it is assumed that the sensible heating load caused by the evapotranspiration of plants on the warmest day of the year will be met by the HP and the latent part is met by the dehumidifier. This is a rational assumption according to the experience of growers in similar facilities [49].

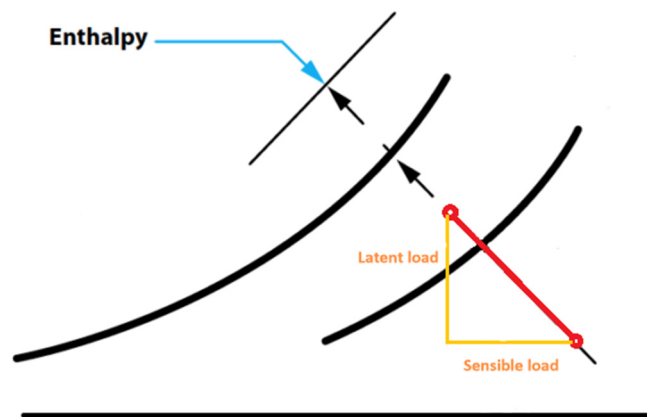


Figure 6. The isenthalpic process of evapotranspiration taken place by humid air.

Total sensible and latent thermal loads of the agrotunnel will be calculated using Equations (11) & (12), respectively.

$$\dot{Q}_{tot,sens} = \dot{Q}_{cc} + \dot{Q}_{sens,inf} + \dot{Q}_{lights} + \dot{Q}_{sens,people} - \dot{Q}_{sens,evap} \quad (11)$$

$$\dot{Q}_{tot,lat} = \dot{Q}_{lat,inf} + \dot{Q}_{lat,people} + \dot{Q}_{lat,evap} \quad (12)$$

The following assumptions are taken into account to run the simulation:

- It is assumed that the growing room and the monitoring room are at the same temperature such that no heat transmission occurs between them.

- It is assumed that the air inside the agrotunnel is uniformly mixed, which is appropriate as the HP locations and clearance over the grow walls ensure paths of airflow.
- The design conditions of agrotunnel are the temperature of 22 °C, and the relative humidity (RH) of 68%.
- The thermal resistance of the still air ($R_{conv,i}$) on the vertical walls is 0.12 m².K/W [44].
- The thermal resistance of the still air ($R_{conv,i}$) on the ceiling is 0.11 m².K/W whenever the indoor temperature is higher than the outdoor temperature, and is 0.16 m².K/W when the indoor temperature is lower than the outdoor temperature [44].
- The thermal resistance of the still air ($R_{conv,i}$) on the floor is 0.16 m².K/W whenever the indoor temperature is higher than the outdoor temperature, and is 0.11 m².K/W when the indoor temperature is lower than the outdoor temperature [44].
- The thermal resistance of the outdoor moving air ($R_{conv,o}$) is 0.029 m².K/W [44].

3.1.5. Maximum Heating Load Model

In order to size HP, the maximum cooling load obtained by CLTD method will be compared to the maximum heating load under the worst-case scenario. The worst-case scenario for heating load estimations is defined for an evacuated agrotunnel, where conduction and convection heat transfer along with the infiltration losses are the only factors included. Total sensible heat loss from the agrotunnel is calculated by Equation (13) in (W or Btu/hr) [44]:

$$\dot{Q}_{sens,heat} = \dot{Q}_{cc,heat} + \dot{Q}_{sens,inf,heat} = \sum \frac{A_k}{R_{tot,k}} (T_i - T_o) + n_{ACH} V_{AT} \rho_a C p_a (T_i - T_o), \quad (13)$$

Total latent heat loss through infiltration is calculated using Equation (7). Accordingly, the maximum total heating load will be calculated by Equation (14):

$$\dot{Q}_{tot,heat} = \dot{Q}_{cc,heat} + \dot{Q}_{sens,inf,heat} + \dot{Q}_{lat,inf,heat} \quad (14)$$

3.1.6. Heat Pump Model

The black box heat pump model is created by utilizing the performance datasheet of GSZ16 Goodman Air-Air Split heat pump (16 SEER and 9 HSPF) for both heating and cooling functions [50]. A supervised regression approach is implemented in Python to derive mathematical functions for the COP (Coefficient of Performance) of heat pumps within a nominal capacity range of 18,000-60,000 BTU/hr. Drawing from Li et al.'s correlations for load demand and COP of an air-conditioning heat pump [51], it is anticipated that the COP regressions would follow a second-degree polynomial pattern based on indoor and ambient temperatures.

3.1.6.1. Heating Mode

The correlation of COP is dependent on the ambient temperature (T_o) in (°C) as Equation (15):

$$COP_{heating} = b_0 + b_1 T_o + b_2 T_o^2, \quad (15)$$

the coefficients $b_0 - b_2$ are extracted using the polynomial curve fitting technique and are shown for all rated capacities of GSZ16 Goodman Heat Pumps in Table 4 for heating mode. The fitting curve of heating COP for 18,000 BTU/hr heat pump is shown in Figure 7a.

Table 4. Coefficients of polynomial correlations of COP in heating mode.

Rated Capacity (Btu/hr)	COP coefficients			
	b_0	b_1	b_2	R^2
18,000	3.202	0.0887	0.000386	99.55
24,000	3.202	0.08879	0.000348	99.53
30,000	3.232	0.09092	-0.00048	99.11

36,000	3.197	0.08875	0.000523	99.66
42,000	3.093	0.0737	0.000217	99.44
48,000	3.273	0.08474	-0.00024	99.13
60,000	2.967	0.07639	0.000272	99.43

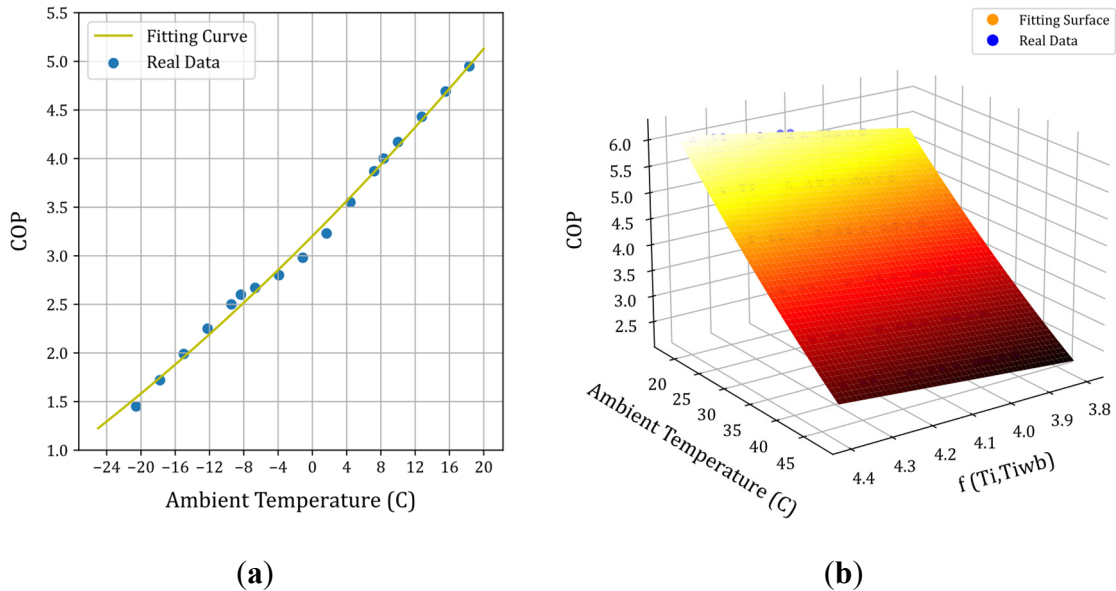


Figure 7. Fitting curves of COP for 18,000 Btu/hr heat pump: (a) heating mode; (b) cooling mode.

3.1.6.2. Cooling Mode

The manufacturer's datasheet for cooling mode were created considering fluctuations in 3 variables (ambient temperature, indoor dry bulb temperature, and indoor wet bulb temperature) [50]. Hence, the regression is carried out in two steps: first, fitting a 2D curve as a function of indoor dry bulb and wet bulb temperatures, second, fitting a 3D surface as a function of first formulation and the outdoor temperature. Figure 6b depicts the fitting surface for the COP of an 18,000 Btu/hr HP in cooling mode. The COP for the cooling mode is determined using Equation (16).

$$\begin{aligned} COP_{cooling} = & b_o + b_1T_i + b_2T_{iwb} + b_3T_o + b_4T_iT_{iwb} + b_5T_iT_o + b_6T_{iwb}T_o + b_7T_i^2 + b_8T_{iwb}^2 + b_9T_o^2 \\ & + b_{10}T_i^2T_o + b_{11}T_{iwb}^2T_o + b_{12}T_iT_{iwb}T_o \end{aligned} \tag{16}$$

Table 5. Coefficients of polynomial correlations of COP in cooling mode.

		Rated Capacity (Btu/hr)						
		18,000	24,000	30,000	36,000	42,000	48,000	60000
Coefficients of COP	b ₀	10.45648	9.14469	10.80332	10.66776	11.1678	10.7799	10.48214
	b ₁	-0.11064	0.012049	-0.13687	-0.12536	-0.14811	-0.12931	-0.12989
	b ₂	-0.21069	-0.21788	-0.18697	-0.19849	-0.208	-0.1978	-0.18888
	b ₃	-0.17693	-0.15915	-0.18717	-0.18142	-0.19111	-0.18515	-0.18156
	b ₄	-0.00038	-5E-05	-0.00024	-0.00012	8.46E-05	-0.00013	-0.00014
	b ₅	0.001363	-0.00014	0.001632	0.001463	0.001723	0.001535	0.001532
	b ₆	0.002596	0.002523	0.002229	0.002317	0.002419	0.002348	0.002227
	b ₇	0.002739	-0.0001	0.003153	0.002864	0.003197	0.002939	0.00295
	b ₈	0.008582	0.008251	0.007745	0.007893	0.00789	0.00791	0.007562

b ₉	0.000623	0.000609	0.000722	0.000671	0.000727	0.000694	0.000706
b ₁₀	-3.4E-05	1.16E-06	-3.8E-05	-3.3E-05	-3.7E-05	-3.5E-05	-3.5E-05
b ₁₁	-0.00011	-9.6E-05	-9.2E-05	-9.2E-05	-9.2E-05	-9.4E-05	-8.9E-05
b ₁₂	7.73E-06	9.2E-07	4.63E-06	2.34E-06	-1.6E-06	2.54E-06	2.61E-06
R ²	99.96	99.98	99.97	99.98	99.98	99.98	99.98

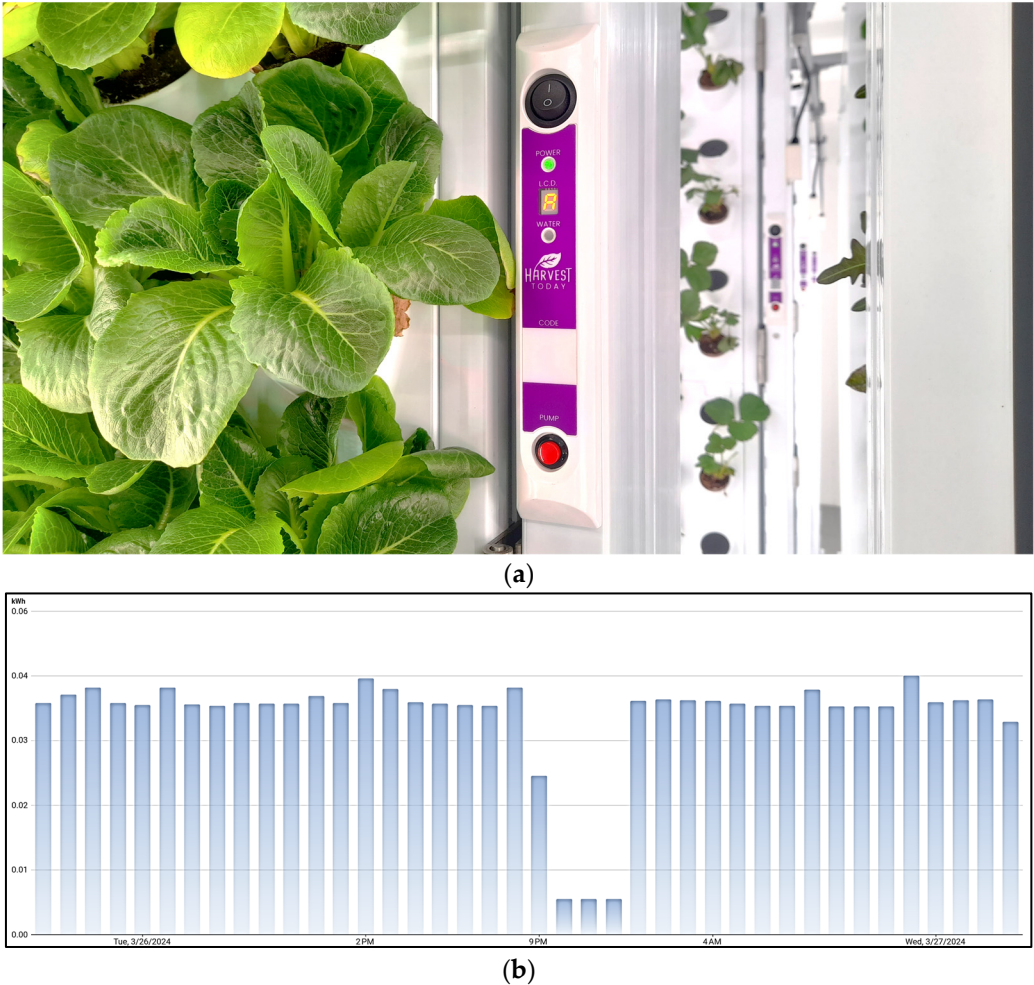
When the maximum heating and cooling load of the agrotunnel on the coldest/warmest day of the year is calculated, the size of HP can be determined. After selecting the HP, its COP correlation is used to calculate the power consumption in kW.

3.2. Electrical Loads

The power demanded by the lighting system and the HPs can be calculated as mentioned in the previous section. The load imposed by the water pumps and dehumidifier is included in this section.

3.2.1. Water Pump

Water pumps are integrated into the grow walls, and they operate 2-4 times per day (1 minute each time) based on the requirements of the plants according to their stage (seedlings or mature). Therefore, the average power consumption of water pumps is reported based on the data recorded by clamp meter [52]. The average power demand by the water pumps is 0.038 kWh, as reported in the data logger (Figure 8).



3.2.2. Dehumidifier

A commercial 23.7 L/day (50 pits/day) refrigerant dehumidifier with the integrated energy efficiency (IEF) of 1.9 L/kWh is being used in cases the heat pump cannot meet the latent load inside the agrotunnel [53]. Based on previous work it is assumed that if the latent load of the agrotunnel is higher than one third (which can be usually provided by HPs) of the maximum sensible load, the rest will be met by dehumidifier [54]. To be conservative, it is considered that all the grow walls are filled with mature plants. Table 6 reports the average water added to each pot of a mature plant during a week, which is measured in the agrotunnel under study. In the basic scenario, it is assumed that all pots are equally allocated for planting four types of crops.

Table 6. Water demand of the mature crops in the agrotunnel (per pot per week).

Crop	Water demand (mL/pot/week)
Kale	315
Lettuce	210
Herbs (Basil, Parsley, Oregano, Mint)	236
Fruits and Vegetables (tomatoes, beans, strawberries)	183

3.3. Solar PV Sizing

PV system sizing was carried out by determining the 1-kW PV potential using the open-source System Advisor Model (SAM) [55] for each of the six locations: Albany, Edmonton, Houston, London, Montreal and San Francisco. Using the total annual electrical energy required for agrotunnel operation ($E_{\text{Annual load}}$ in (kWh)) in each location and the annual energy potential of 1-kW PV system determined from SAM ($E_{\text{Annual load, 1kW}}$ in (kWh)), the total PV system size ($PV_{\text{Sys.Capacity}}$) required to meet the annual electrical load is ascertained. The formula for the determining the PV size in (kW) is given by Equation (17):

$$PV_{\text{Sys.Capacity}} = \frac{E_{\text{Annual Load}}}{E_{\text{Annual Load, 1kW}}} \quad (17)$$

The PV system capacity determined through the estimate calculation is then used as input in SAM to run a detailed simulation at the appropriate scale. The simulations are run for each location and double checked if they meet the annual electrical load of the agrotunnel. Additionally, the land area required for PV systems, considering their modules' transparency levels ranging from 0% (conventional silicon modules) to 69% (semi-transparent modules) will be reported. Table 7 details the assumptions used to perform the final modelling in SAM. A novel fixed-tilt racking design, adaptable into a variable-tilt racking system [15], is considered for use in this research. Soiling losses, DC power losses and AC power losses are kept as default.

Self-consumption (SC) and self-sufficiency (SS) are important metrics for assessing the energy performance of distributed energy systems at the local level [56]. SC measures the proportion of locally produced energy that is consumed locally, calculated as the energy generated by the PV system (E_{PV}) minus the energy sent to the grid ($E_{\text{to grid}}$), divided by the total energy generated by the PV system (E_{PV}) as seen in Equation 18. SS, on the other hand, indicates the extent to which local energy production meets local energy demand, calculated as the energy generated by the PV system minus the energy sent to the grid, divided by the local energy consumption (E_{load}) (Equation 19). Both metrics exclude nighttime hours when the PV system is not operational, and all energy is sourced from the grid, thus SC and SS are set to zero during these times. These metrics can be formulated through Equations (18) & (19) [57,58].

$$SC = \frac{E_{\text{PV}} - E_{\text{to grid}}}{E_{\text{PV}}} \times 100 \quad (18)$$

$$SS = \frac{E_{PV} - E_{togrid}}{E_{Load}} \times 100$$

(19)

Table 7. Input parameter for SAM for PV system sizing for the agrotunnel.

Parameters	London	Albany	Edmonton	Houston	Montreal	San Francisco
PV module	Heliene 144HC-460 Bifacial [59]					
Module type	Mono Crystalline Silicon - Bifacial					
Tilt angle	34° [60]	34° [61]	53° [62]	27° [63]	30° [64]	32° [65]
Azimuth	180°					
Soiling losses	5%					
DC Power losses	4.44%					
AC Power losses	1%					

3. Results

The assessment of thermal loads will account for the impact of various geographical locations, including London, ON; Montreal, QC; Edmonton, AB; Albany, NY; San Francisco, CA; and Houston, TX. Additionally, a sensitivity analysis will be performed to examine the effects of key variables such as envelope thermal resistance, number of lights, crop type, and indoor design conditions.

3.1. Validation

The methodology for both the CLTD and the maximum heating requirement model is validated against the results obtained from HAP. For the minimum dry bulb and wet bulb ambient temperatures of -19.4 °C and -20.22 °C, respectively, and the maximum dry bulb and wet bulb ambient temperatures of 29.44 °C and 21.67 °C, respectively, the heating and cooling loads of the AT in London, Ontario, Canada will be obtained using current model, as shown in Figure 9. According to this figure, the average deviation of calculated heating and cooling loads from the HAP simulation results is 5.0 % and 4.3 %, respectively. The present model provides more conservative results for sizing the HVAC systems.

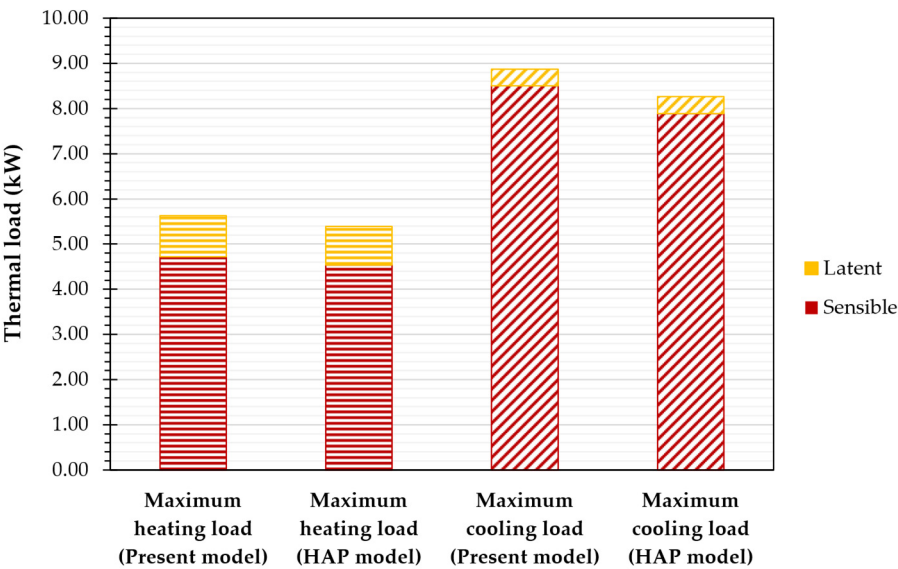


Figure 9. The results of the present model vs those of HAP model for calculation of heating and cooling loads.

Likewise, the HP model's verification involves comparing it with the manufacturer datasheet of the GSZ16 series Goodman Air-Air heat pump. The average variance of the matched outcomes for heating COP with the manufacturer's datasheet is determined to be 2.48%. Meanwhile, the average variance of the matched outcomes for cooling COP stands at 1.26%.

The total power demand of the agrotunnel has been verified using data recorded by a power clamp meter. Recording began in mid-February 2024, and as of mid-June 2024, data is available for March, April, and May 2024. March data, however, showed inconsistencies in both the climatic conditions of the agrotunnel and the data recording procedure. Therefore, the monthly power consumption of the entire system has been verified according to the conditions of April and May, reported in Table 8. Figure 10 illustrates the similarity between the modeling results and the recorded data, with an error ranging from 5.5% to 7.5%. The sources of error include real-world operational variations such as changes in planted crop types, RH setpoints, and the number of operating lights as experiments are adjusted. Additionally, temporary additions or removals of some equipment, such as water transfer pumps, contribute to these variations. Despite these factors, the current model tends to overestimate the total energy required, making it a more conservative estimate.

Table 8. Conditions considered in the experimental verification of monthly total power demand.

Conditions	Values	
	April	May
Number of BGL180A lights	28-32	32
Number of BGL180C lights	2	2
Temperature (°C)	20	19.5
RH (%)	59	55
Ambient conditions	London, ON Airport meteorological data [66]	London, ON Airport meteorological data [66]

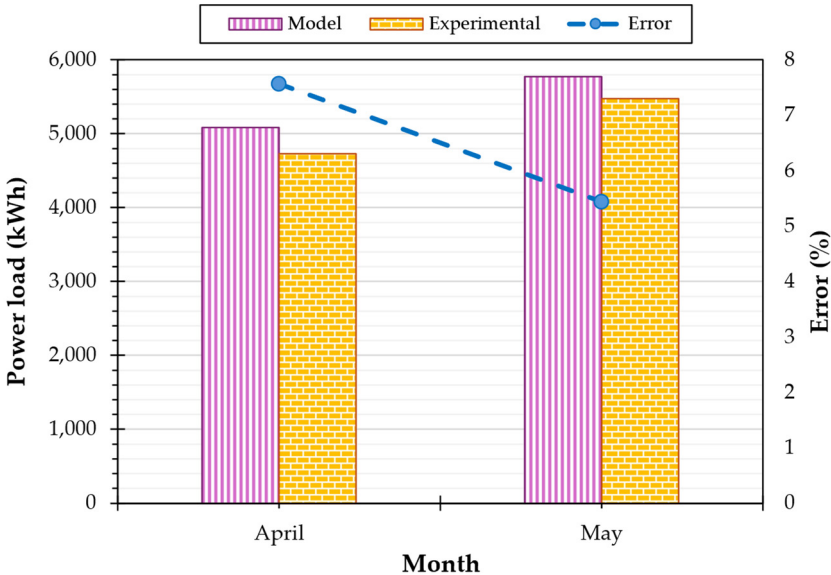


Figure 10. Monthly power demand of the agrotunnel reported for April and May 2024 (modeling vs. experimental data).

3.2. Thermal/Electrical Load Analysis

Initially, the year-round heating and cooling load of the agrotunnel is simulated based on the climatic conditions of the six selected case study locations. This section evaluates solely the sensible

and latent loads induced by envelope transmission and infiltration, aiming to compare the impact of geographic location while disregarding constant thermal loads such as people, crops, and lights. Figure 11 illustrates the results of this comparison. As can be seen in Figure 11, Edmonton exhibits the highest total load (sensible heating load of 9,370 kWh, latent heating load of 38,035 kWh, and the sensible cooling load of 603.5 kWh), whereas San Francisco displays the lowest (sensible heating load of 2,255 kWh, latent heating load of 36,680.5 kWh, and the sensible cooling load of 1050.5 kWh), which aligns with their distinct climates as expected. San Francisco's climate during the year undergoes less fluctuations such that the microclimate of the agrotunnel located there will have the least deviation from the outdoor conditions. Cities with the highest sensible heating loads demonstrate the lowest sensible cooling loads, and vice versa. Notably, a significant portion of the load corresponds to latent heating resulting from the humidity ratio difference between the agrotunnel and the exterior. This underscores the importance of maintaining this humidity level as a crucial HVAC measure.

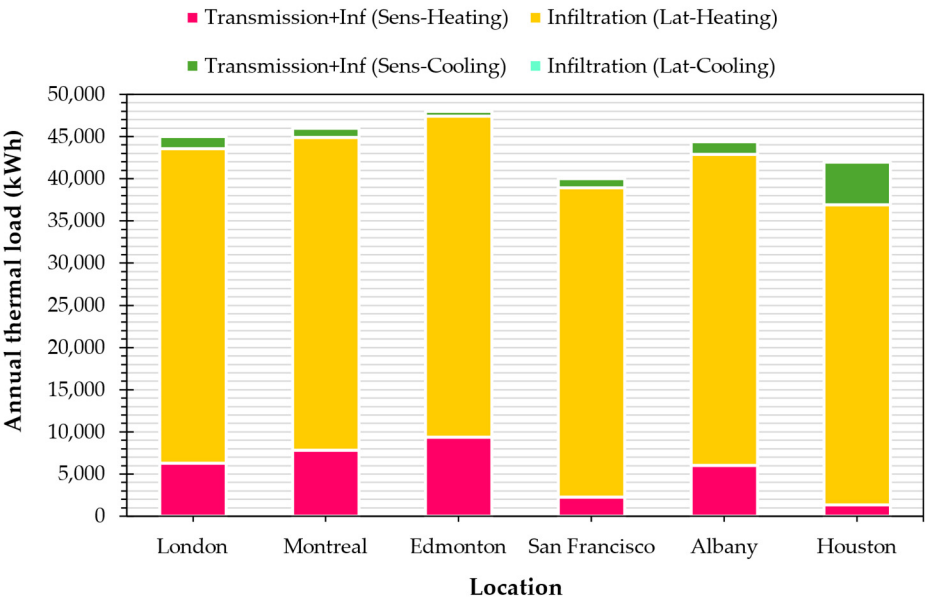


Figure 11. Heating and cooling loads caused by heat transfer through the agrotunnel envelope and the infiltration.

Figure 12 illustrates the proportion of each heat transfer component of the individual thermal loads in an agrotunnel located in London, ON. It is evident that lights account for 40% of the thermal loads in the agrotunnel. Following closely, the evapotranspiration of plants places a substantial burden on the HVAC systems within the structure (32%). Sensible infiltration and wall transmission account for roughly a quarter of the load and finally the load imposed by the presence of the people has almost no impact.

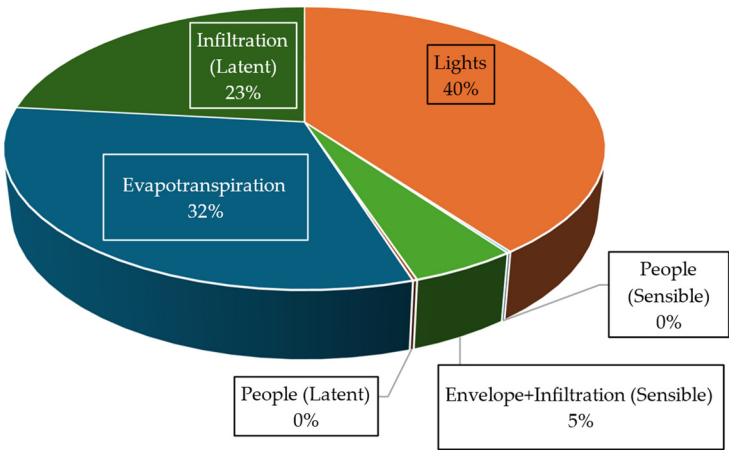


Figure 12. Share of heat transfer components in the annual thermal load of the agrotunnel in London, ON.

The heat pumps are sized and selected based on the worst-case scenario, encompassing either the maximum cooling or heating load within the building as illustrated in Figure 13. The considerable variance between the maximum heating and cooling loads, resulting in potential oversizing of the HP, is due to the definition of the worst-case scenario on the coldest day (evacuated agrotunnel devoid of plants and lights). This can be a subject for future deliberation in decision-making processes as it is only necessary to ensure heating to keep plants alive. The disparity between the heat pump's size and the maximum heating load stems from commercially unavailable HP capacities. This indicates a market opportunity for more refined HP sizing to allow for closer optimizations. The largest HP capacity is designated for an agrotunnel situated in Edmonton (11 kW or 36,000 Btu/hr), while the smallest is allocated for structures in San Francisco and Houston (7 kW or 24,000 Btu/hr).

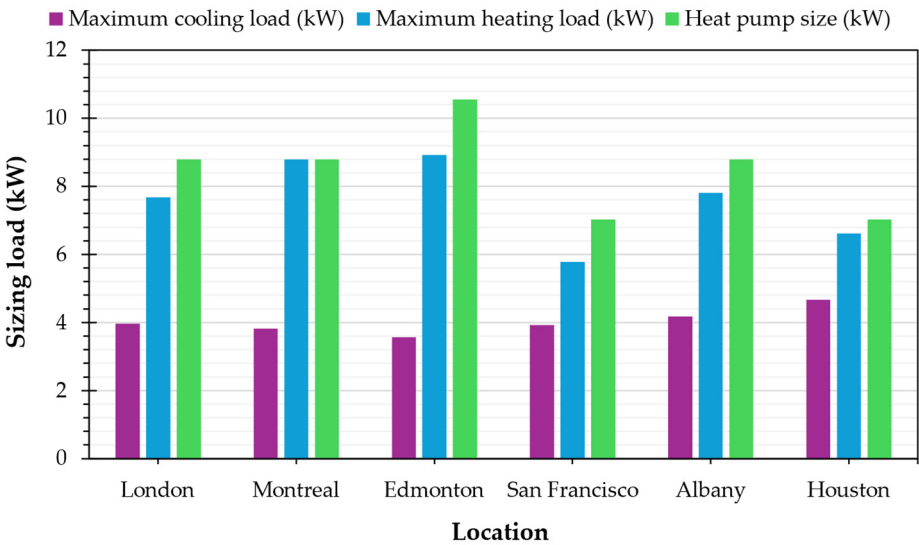


Figure 13. The thermal load of the agrotunnel under worst-case scenario and HP sized to meet the maximum loads.

In the subsequent stage, Figure 14 presents projections of the annual electricity required by four primary components: lights, HP, dehumidifier, and pumps, across three cities with varying levels of demand. Across all three locations, the highest power demand is attributed to the artificial lighting system, followed by the dehumidifier, with the pumps requiring the least power. In Edmonton, where the heating demand of the agrotunnel notably surpasses the cooling demand (as depicted in Figure 11), the HVAC system necessitates less power to cater to the cooling load of the structure.

Additionally, the lighting system not only fulfills the heating requirement but also generates surplus cooling load, even on cold days. Consequently, the net value of HP power consumption during cold days is even smaller (2,756 kWh, 4%). In conclusion, it can be argued that the colder the climate, the lower the predicted demand for the HVAC system within the current system design.

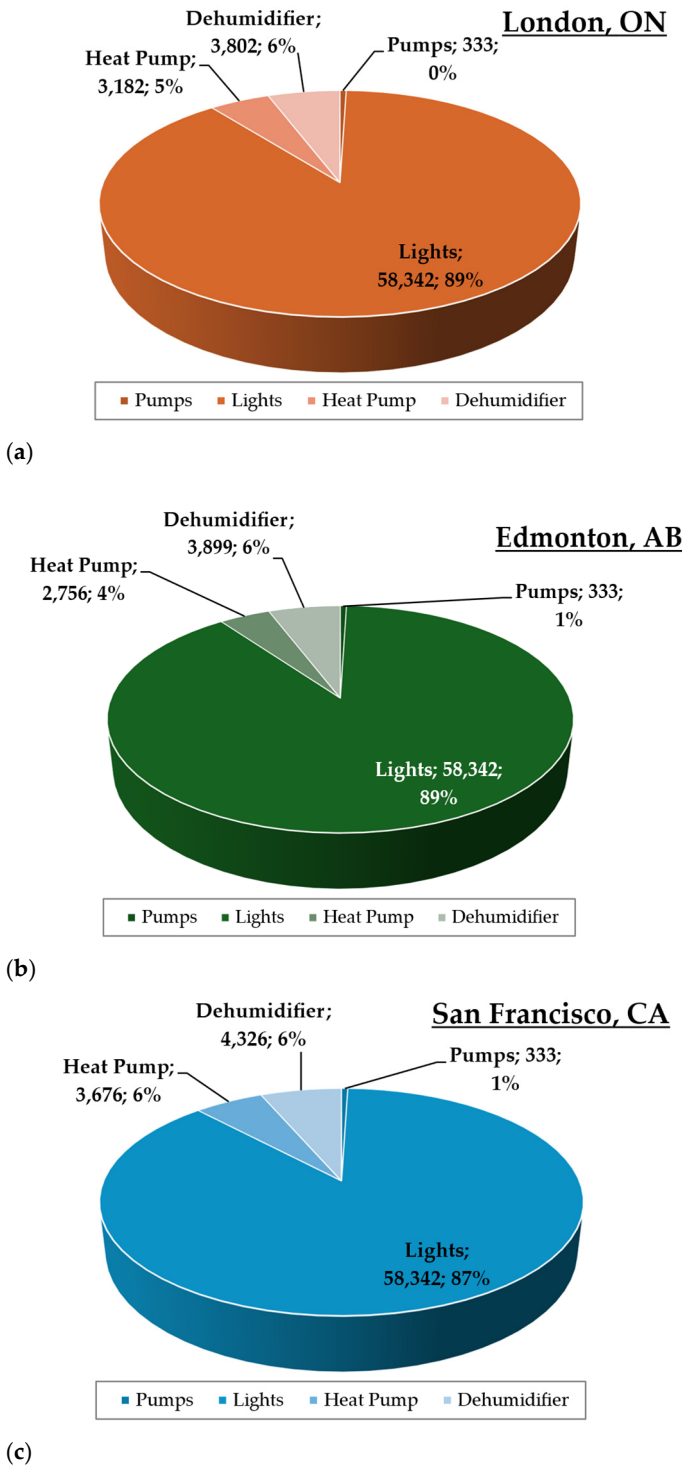


Figure 14. The annual electricity power demand of electrical equipment in the agrotunnel (kWh).

3.3. Sensitivity Analysis

In this section, the sensitivity of two major energy indices (annual thermal load and annual power demand) are studied under the influence of the most significant parameters' variations. The hourly thermal load requirements of the agrotunnel are first portrayed in Figure 15 for the year-round

application. As a result of the continuous operation of lights, the building experiences a need for cooling throughout the year.

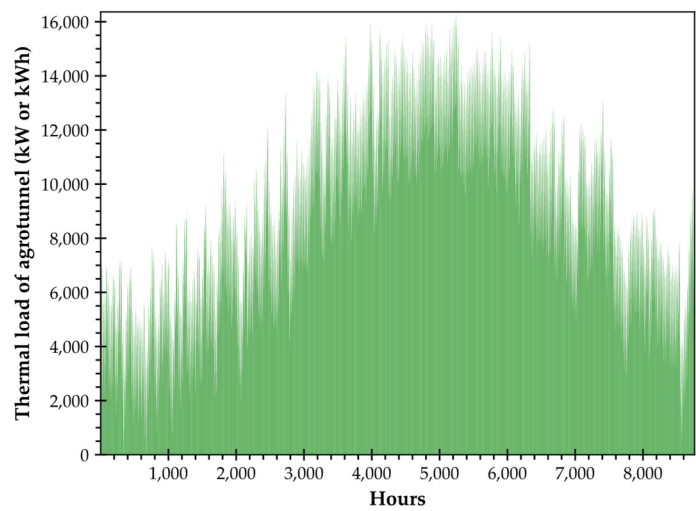


Figure 15. The year-round hourly thermal load of the agrotunnel.

The choice of crop to be harvested in an agrotunnel is greatly influences the water usage, as it directly impacts the evapotranspiration rate and consequently alters the load of the building. According to Figure 16, any variation in the evapotranspiration rate of the plants results in a consistent thermal load, as evapotranspiration is an isenthalpic process. There is, however, a reduction in power demand due to changes in the electricity consumption rate of dehumidifiers, resulting from a significant decrease in the latent load of the agrotunnel.

According to Figure 16, in an agrotunnel dedicated solely to growing kale, which requires more frequent watering cycles, there is a 25.53% increase in annual electricity demand compared to an agrotunnel for growing some specific herbs (from 65.46 MWh to 82.42 MWh). This difference rises to 32.26% and 34.32% when compared to specific vegetables and lettuce, respectively.

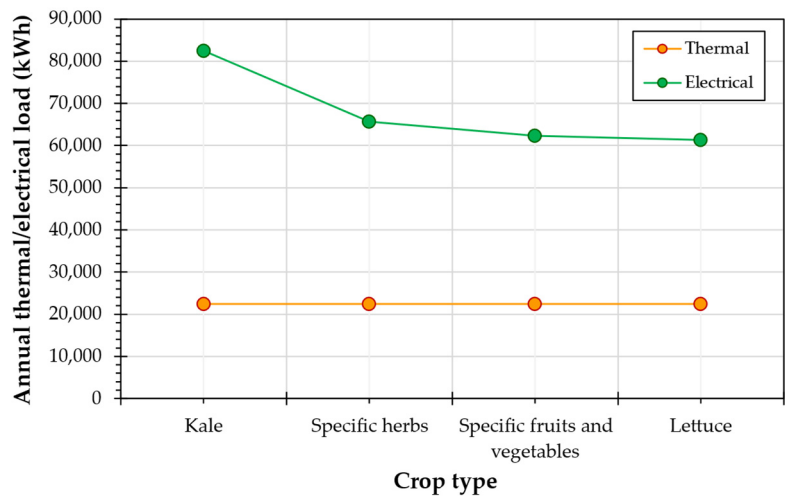


Figure 16. Variation in annual thermal and electrical loads of the agrotunnel vs change in crop type based on water use in grow walls for each specific crop type.

Figure 17 illustrates the variations in the annual thermal and electrical loads of the agrotunnel concerning changes in the photoperiod. According to Figure 17, reducing the photoperiod from 24 to 14 hours per day, a practice commonly applicable to many crops [67], results in a substantial decrease

in the annual electrical load, dropping from 65,658 kWh to 37,711 kWh, which was normally expected due to the reduction in the power load imposed by the lights. The annual thermal load, however, has a different trend. It decreases from 23,497 kWh to 16,533 kWh with the reduction in the photoperiod from 14 to 22 hours per day. In a northern climate like London, ON, it is expected to have significant heating load rather than cooling load for an evacuated agrotunnel. Increasing the photoperiod will assist in providing the heating load of the building by lights' dissipated energy. In other words, increasing the period, in which the lights are on will neutralize the heating load of the agrotunnel. For photoperiods more than 22 hours, the cooling load imposed by the lights will show up such that, the decreasing trend in the annual thermal load of the agrotunnel will be converted to an increasing approach. Hence, optimization procedure on the influence of photoperiod on the annual thermal demands should be taken into account, especially for case the thermal demand is supplied by the conventional non-electrical sources.

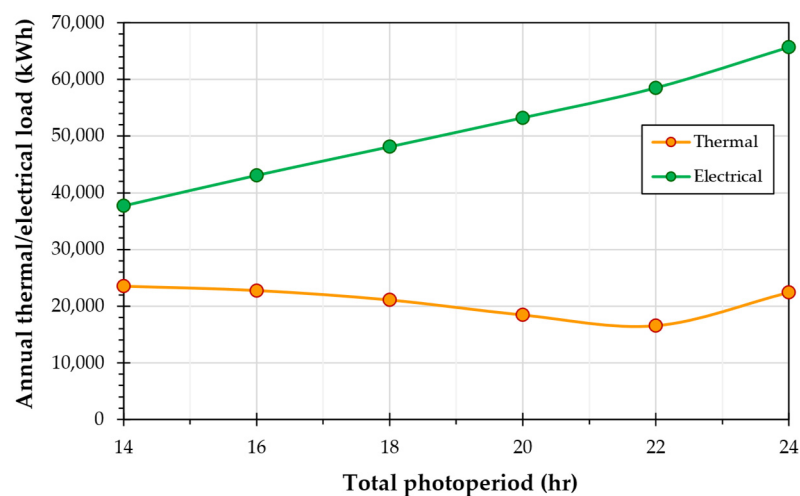


Figure 17. Variation in annual thermal and electrical loads of the agrotunnel vs change in the total photoperiod.

In Figure 18, it is evident that increasing the design temperature of the agrotunnel from 18 to 24 °C leads to a notable decrease in the building's annual thermal loads, dropping from 36,942 to 13,573 kWh. This reduction primarily stems from decreased cooling demands. Consequently, the annual electrical load is expected to decrease from 74,811 to 67,943 kWh due to a drop in the electrical load of HP and dehumidifier. Notably, the design temperature emerges as a crucial parameter, significantly influencing both the thermal (with a sensitivity of 63.26%) and electrical (with a sensitivity of 19.05%) loads of the agrotunnel.

The impact of the building's thermal resistance is investigated, with findings outlined in Figure 19. Analysis reveals that variations in the thermal resistance of the agrotunnel's walls, ranging from 2.8 to 5.8 W/m².K, do not yield significant changes in the thermal and electrical loads of the building. This observation suggests that factors such as lighting, evapotranspiration, and infiltration, as demonstrated in Figure 12, primarily dictate the thermal/electrical loads. Consequently, the thermal resistance parameter is not included among the influential variables.

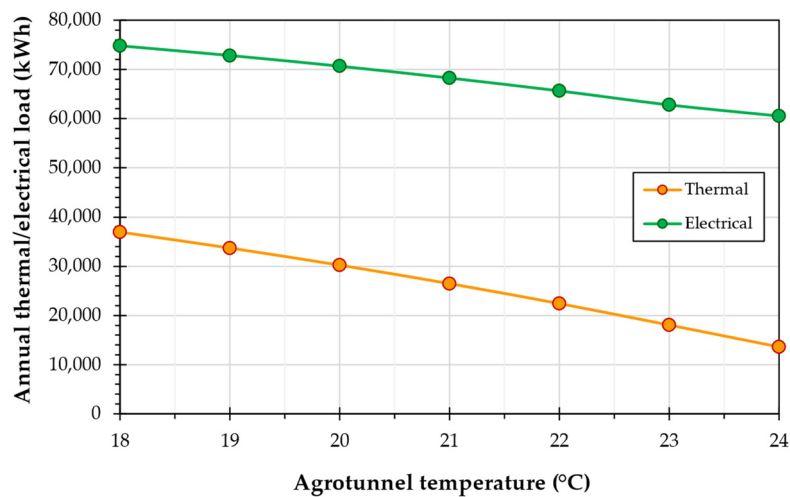


Figure 18. Variation in annual thermal and electrical loads of the agrotunnel vs change in the agrotunnel’s design temperature.

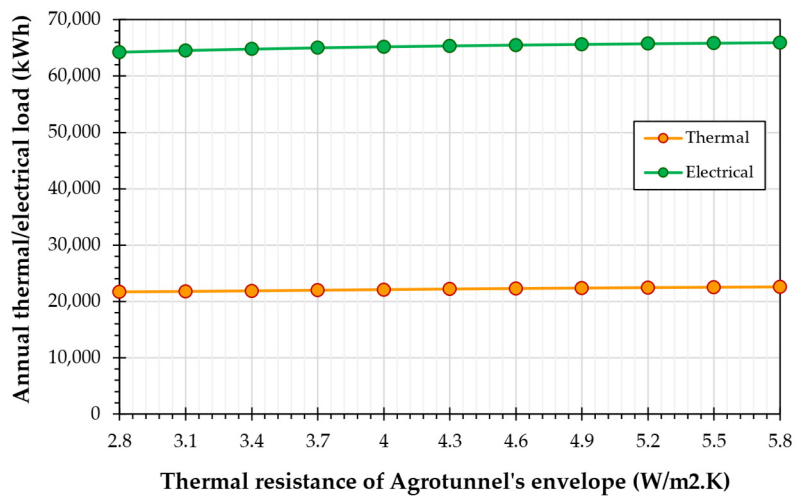


Figure 19. Variation in annual thermal and electrical loads of the agrotunnel vs change in the thermal resistance of the agrotunnel’s envelope.

3.4. PV System Sizing

The annual electrical energy requirements of the agrotunnel for the six locations are given in Table 9. According to Table 9, colder regions have lower energy requirements compared to warmer regions. This is because the excess heat generated by lights compensates for the heating needs imposed by the outdoor environment.

Table 9. Annual electrical energy requirements for the agrotunnel.

Location	Annual electrical energy required (kWh)
London	65,658
Albany	65,769
Edmonton	65,313
Houston	68,461
Montreal	65,899
San Francisco	66,676

The SAM results including the PV system size and the annual electrical energy generation for the six locations are detailed in Table 10.

Table 10. PV system size for the agrotunnel.

Location	London	Albany	Edmonton	Houston	Montreal	San Francisco
Number of modules	104	103	104	96	102	89
DC power rating (kW)	47.86	47.40	47.86	44.18	46.94	40.96
DC to AC ratio	0.96	0.95	0.96	0.88	0.94	1.03
Annual electrical energy generation (kWh)	65,814	65,840	65,372	68,861	66,457	67,145

The bar graph in Figure 20 depicts the annual electrical energy required and produced by the associated PV systems for all the six locations. The chart clearly indicates that the net-zero approach has been achieved for all locations. The similar sizes of PV systems confirm that the agrotunnel's performance is not sensitive to its location, particularly in northern climates. The smallest PV system size is needed in San Francisco (41.42 kW). Interestingly, the annual electrical output from the system in San Francisco comes out to be higher than London, Montreal, Edmonton and Albany since the electrical energy generation potential is higher in San Francisco (1641.5 kWh/kW) due to the higher level of solar irradiation there.

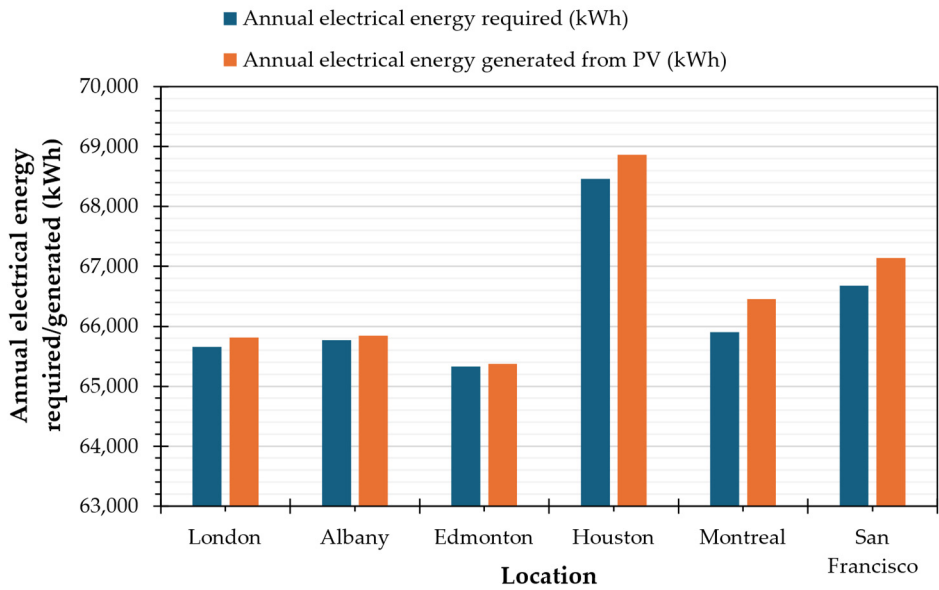


Figure 20. Annual electrical energy required and generated for all the six locations.

Figure 21 illustrates how the total land area used for PV installations changes with increasing module transparency. The data obtained from SAM for all locations are detailed in Table 11. A notable point in Figure 21 concerns the land required for PV system installations in Edmonton. Due to the high interrow spacing necessary to avoid shading, the total land area used for the PV system in Edmonton is considerably larger compared to other locations.

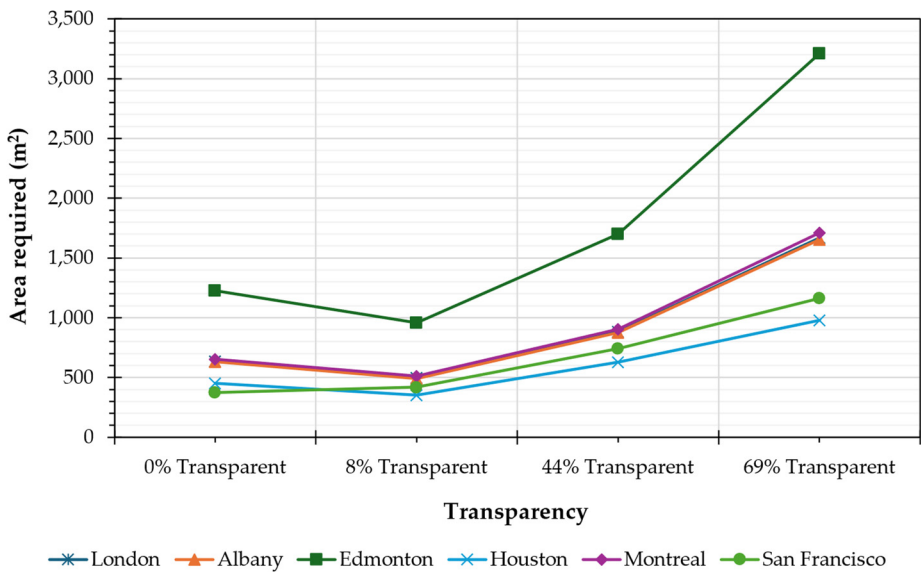


Figure 21. Variations of land area required for PV systems with respect to the variations in the transparency of PV modules.

Table 11. Total land area required for PV system installations.

Location	Transparency				
	PV system size (kW)	0%	8%	44%	69%
London	47.86	637	497	883	1669
Albany	47.40	631	492	875	1653
Edmonton	47.86	1226	956	1699	3211
Houston	44.18	453	353	627	979
Montreal	46.94	654	510	906	1712
San Francisco	40.96	373	418	743	1161

Table 12 presents the SC and SS values for the six locations under study. Despite the higher electrical energy demand in warmer regions, such as Houston, the PV system capacity required to supply the agrotunnel is smaller. This results in higher SC and SS values due to the adequate solar irradiation levels. Among the cold regions, London, ON exhibits the highest SC and SS values.

Table 12. Self-Consumption and Self-Sufficiency values for different locations.

Location	Self-Consumption (%)	Self-Sufficiency (%)
London	37.33	37.42
Albany	37.61	37.65
Edmonton	36.02	36.04
Houston	39.66	39.89
Montreal	36.93	37.24
San Francisco	31.97	32.19

Figure 22 illustrates the monthly variations in SC and SS values over 12 months in London, ON. Figure 22 shows that SC and SS values exhibit opposite behaviors: SC increases when the electrical load exceeds the generation capacity of the PV system (e.g., in winter), whereas SS rises when the electrical demand is below the PV system's total energy capacity (e.g., in summer).

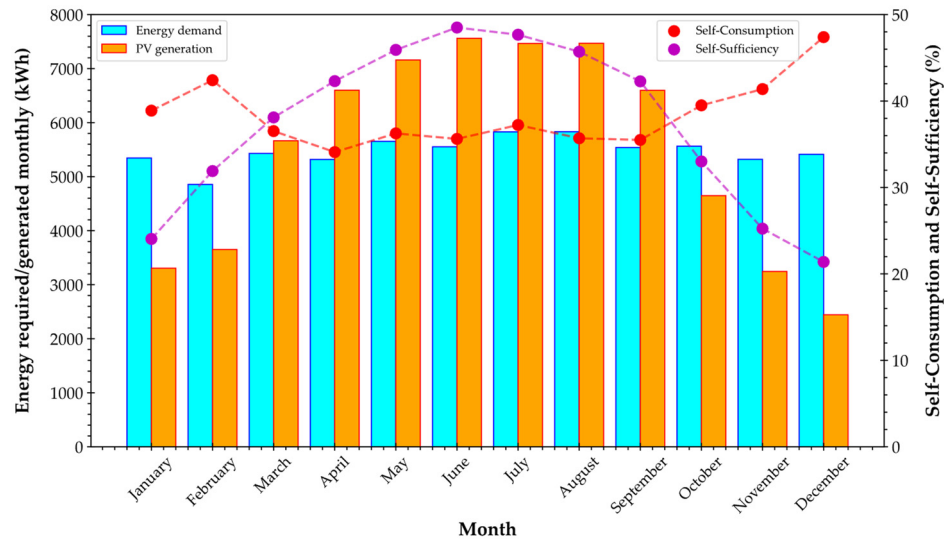


Figure 22. Monthly variations of Self-Consumption and Self-Sufficiency of PV system designed for London, ON.

Figure 23 demonstrates that the electrical energy demand of the agrotunnel remains relatively consistent throughout the year, while the energy generated by the PV system fluctuates with variations in solar irradiation. To improve the compatibility between the load and the generated energy, and thereby increase the SS of the system, the use of electrical or thermal batteries can be considered.

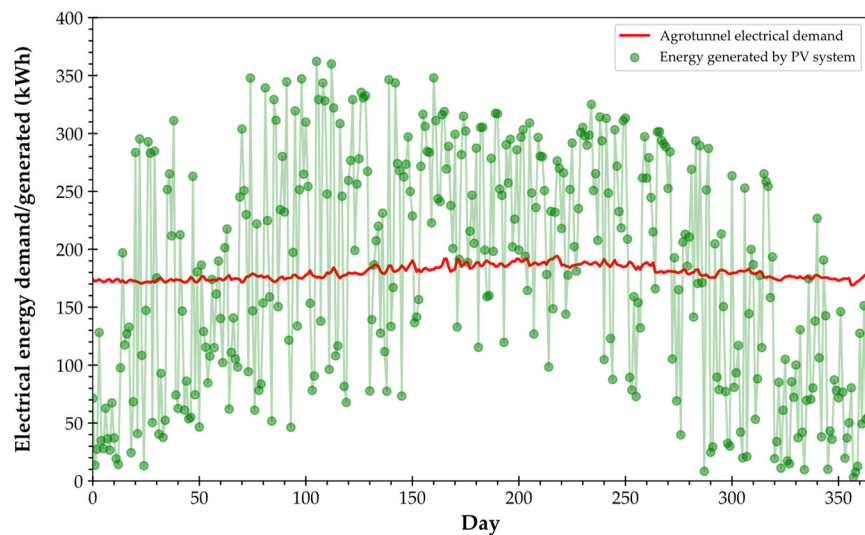


Figure 23. Variations of daily electrical energy demand and daily energy generated by PV system over a year in London, ON.

4. Discussion

This study provides valuable insights into the feasibility of agrivoltaic agrotunnels. The PV sizes, ranging from 41.42 kW to 48.32 kW across locations with significantly different climates, indicate that the agrotunnel is not highly sensitive to location and climatic conditions. For conventional opaque PV modules, the required installation land area is 373 m² in San Francisco, 453 m² in Houston, 631 m² in Albany, 637 m² in London, 654 m² in Montreal, and 1,226 m² in Edmonton. For an agrotunnel with a total surface area of 117 m², the PV land index (total land area required by PV system to the total

surface area of agrotunnel) is as follows: 3.2 m²/m² for San Francisco, 3.87 m²/m² for Houston, 5.39 m²/m² for Albany, 5.44 m²/m² for London, 5.59 m²/m² for Montreal, and 10.48 m²/m² for Edmonton. The solar flux level, commercial availability of PV modules and the interrow spacing alter the values for each location. The land requirements increase for systems with semi-transparent modules with transparencies of 8%, 44%, and 69%.

By utilizing single-axis tracking PV systems on just 1% of the total agricultural lands in Ontario, Quebec, and Alberta [68], it is possible to establish 231,167, 220,944, and 534,334 agrotunnels in these regions, respectively. This demonstrates the potential of this technology to enhance food security, especially in areas with harsh climates where local food production is challenging and energy, operation, and transportation costs are high [69]. In grid-tied conventional formats, the high capital costs of indoor farming facilities and the vertical farming industry [70] have deterred many investors [71], leading to farm closures, asset sales, loan defaults, and company bankruptcies [72–81]. Some industry giants, operating multiple industrial-scale farms with significant funding, have gone bankrupt after 20 years [82], and many startups have failed due to high operational costs and lower-than-expected crop yields [83,84]. In this context, becoming less dependent from/on the electricity grid by using affordable renewable energy sources, such as PV technology, can help many companies survive. For this, an open-source thermal-electrical model has been developed in the current study for predicting the energy demands of a semi-commercial scale indoor vertical farming facility, the agrotunnel. The model has been validated using commercial software, industrial datasheets, and real-time data from the agrotunnel, making it reliable and applicable to various locations. Investors and farmers can use this model and the findings of this research to evaluate the energy requirements of indoor farming, thereby investing in such technologies with greater confidence. With the PV systems sized appropriately as shown here agrivoltaics agrotunnel investors are completely insulated from electricity price fluctuations. Similarly, when compared to competitors that use natural gas for heating, the agrivoltaics agrotunnel economics are not impacted by natural gas fluctuations. An upfront cost in solar PV, means that all operational energy for 25 years on the agrivoltaics agrotunnel is known and paid for via financing.

The open-source model provided in this study is available for researchers worldwide to assess, modify, and upgrade to address its limitations. Currently, the model only considers the plug loads in the agrotunnel. Safety factors must be incorporated for future potential loads. The heat pump model can be enhanced from a black-box model to a thermodynamic model, increasing compatibility with various conditions and environmental limitations. Additionally, a comprehensive economic model should be developed to compare capital, labor, and energy costs. Future economic investigations will offer more valuable insights for farmers and investors.

5. Conclusions

This study developed and validated a thermal-electrical model to size a net-zero agrivoltaics array for an agrotunnel. It incorporated wall transmission, infiltrations, and plant evapotranspiration, sized heat pumps for temperature control, and measured plug loads such as water pumps, LED lighting, and dehumidifiers. Thermal analysis showed that in an agrotunnel in London, ON, lights contributed 40% of the thermal load, while plant evapotranspiration added 32%. Sensible infiltration and wall transmission together accounted for about 25% of the load, and the presence of people had a negligible impact on the thermal load.

The choice of crop in an agrotunnel significantly impacts water usage and building load due to varying evapotranspiration rates. Although the thermal load remains consistent because evapotranspiration is isenthalpic, power demand decreases as dehumidifier electricity consumption drops with reduced latent load. For example, growing kale, which requires frequent watering, increased annual electricity demand by 25.53% compared to herbs (Basil, Parsley, Oregano, and Mint), and by 32.26% and 34.32% compared to vegetables and fruits (tomatoes, beans, and strawberries) and lettuce, respectively. Reducing the photoperiod from 24 to 14 hours per day significantly decreased the annual electrical load of an agrotunnel from 65,658 kWh to 37,711 kWh, primarily due to reduced lighting power. In colder climates, extended photoperiods helped offset

heating demands due to lights' dissipated energy. Hence, optimizing photoperiods is crucial, especially when conventional non-electrical sources supply thermal demands. Moreover, the design temperature was a crucial parameter, strongly influencing both thermal (63.26% sensitivity) and electrical (19.05% sensitivity) loads.

The agrotunnels located in colder regions have lower annual electrical energy requirements compared to those in warmer regions. This is because the excess heat generated by the lights offsets the heating needs caused by the outdoor environment. According to the results, the net-zero approach was achieved for the annual electrical energy requirements and production from PV systems across six locations (London, Montreal, Edmonton, Albany, San Francisco, and Houston). Albany required the largest PV capacity at 48.32 kW to meet its annual energy demand of 67,497 kWh. Conversely, San Francisco needed the smallest system size at 41.42 kW. Notably, San Francisco's PV system generates more electricity annually than London, Montreal, Edmonton, and Albany due to its higher solar irradiation, yielding 1641.5 kWh/kW. The PV system capacity for an agrotunnel in warmer regions such as Houston was smaller due to ample solar irradiation. Consequently, these regions showed higher SC and SS values. London, ON, among the colder regions, exhibited the highest SC and SS values overall. Evaluating the monthly trend of SC and SS values proved that they behave oppositely: SC increased during months when electrical demand surpassed PV system generation capacity (e.g., winter), while SS rose when demand fell below the PV system's energy capacity (e.g., summer).

Supplementary Materials: The following supporting information can be downloaded at: <https://osf.io/sdt74/files/osfstorage>

Author Contributions: Conceptualization, J.M.P.; methodology, N.A., U.J. and J.M.P.; software, N.A., U.J. ; validation, N.A., U.J. and J.M.P ; formal analysis, N.A., U.J. and J.M.P ; investigation, N.A., U.J.; resources, J.M.P.; data curation, N.A., U.J. ; writing—original draft preparation, N.A., U.J. and J.M.P ; writing—review and editing, N.A., U.J. and J.M.P ; visualization, N.A., U.J. ; supervision, J.M.P.; project administration, J.M.P.; funding acquisition, J.M.P.. All authors have read and agreed to the published version of the manuscript.

Funding: This work was supported by the Weston Family Foundation through the Homegrown Challenge, Carbon Solutions @ Western and the Thompson Endowment.

Institutional Review Board Statement Not applicable.

Informed Consent Statement: Not applicable.

Data Availability Statement: Data for this manuscript is available at:

Acknowledgments: The authors would like to thank Greg Whiteside and Jeremy Van Maar for helpful discussion and technical assistance.

Conflicts of Interest: The authors declare no conflicts of interest.

References

1. US EPA, O. Global Greenhouse Gas Overview Available online: <https://www.epa.gov/ghgemissions/global-greenhouse-gas-overview> (accessed on 19 June 2024).
2. Beacham, A.M.; Vickers, L.H.; Monaghan, J.M. Vertical Farming: A Summary of Approaches to Growing Skywards. *The Journal of Horticultural Science and Biotechnology* **2019**, *94*, 277–283, doi:10.1080/14620316.2019.1574214.
3. Plants | Free Full-Text | Indoor Vegetable Production: An Alternative Approach to Increasing Cultivation Available online: <https://www.mdpi.com/2223-7747/11/21/2843> (accessed on 19 June 2024).
4. Sadek, N.; kamal, N.; Shehata, D. Internet of Things Based Smart Automated Indoor Hydroponics and Aeroponics Greenhouse in Egypt. *Ain Shams Engineering Journal* **2024**, *15*, 102341, doi:10.1016/j.asej.2023.102341.
5. The Transformative Environmental Effects Large-Scale Indoor Farming May Have On Air, Water, and Soil - Eric W. Stein, 2021 Available online: <https://journals.sagepub.com/doi/full/10.1177/1178622121995819> (accessed on 19 June 2024).

6. Mitchell, C.A. History of Controlled Environment Horticulture: Indoor Farming and Its Key Technologies. *HortScience* **2022**, *57*, 247–256, doi:10.21273/HORTSCI16159-21.
7. Ahamed, M.S.; Sultan, M.; Monfet, D.; Rahman, M.S.; Zhang, Y.; Zahid, A.; Bilal, M.; Ahsan, T.M.A.; Achour, Y. A Critical Review on Efficient Thermal Environment Controls in Indoor Vertical Farming. *Journal of Cleaner Production* **2023**, *425*, 138923, doi:10.1016/j.jclepro.2023.138923.
8. Sheibani, F.; Bourget, M.; Morrow, R.C.; Mitchell, C.A. Close-Canopy Lighting, an Effective Energy-Saving Strategy for Overhead Sole-Source LED Lighting in Indoor Farming. *Front. Plant Sci.* **2023**, *14*, doi:10.3389/fpls.2023.1215919.
9. Hachem-Vermette, C.; MacGregor, A. Energy Optimized Envelope for Cold Climate Indoor Agricultural Growing Center. *Buildings* **2017**, *7*, 59, doi:10.3390/buildings7030059.
10. Avgoustaki, D.D.; Xydis, G. Indoor Vertical Farming in the Urban Nexus Context: Business Growth and Resource Savings. *Sustainability* **2020**, *12*, 1965, doi:10.3390/su12051965.
11. Despommier, D. Vertical Farms, Building a Viable Indoor Farming Model for Cities. *Field Actions Science Reports. The journal of field actions* **2019**, 68–73.
12. George, P.; George, N. Hydroponics-(Soilless Cultivation of Plants) for Biodiversity Conservation. *Int. J. Mod. Trends Eng. Sci* **2016**, *3*, 97–104.
13. Pinstруп-Andersen, P. Is It Time to Take Vertical Indoor Farming Seriously? *Global Food Security* **2018**, *17*, 233–235, doi:10.1016/j.gfs.2017.09.002.
14. Walling, M. As Indoor Farming Startups with Hundreds of Millions in Funding Head to Bankruptcy, Critic Says: “Boy, This Is a Dumb Idea” Available online: <https://fortune.com/2023/09/18/indoor-farming-startups-bankruptcy-dumb-idea-expensive/> (accessed on 29 March 2024).
15. Vandewetering, N.; Hayibo, K.S.; Pearce, J.M. Open-Source Design and Economics of Manual Variable-Tilt Angle DIY Wood-Based Solar Photovoltaic Racking System. *Designs* **2022**, *6*, 54, doi:10.3390/designs6030054.
16. Fu, R.; Feldman, D.J.; Margolis, R.M. US Solar Photovoltaic System Cost Benchmark: Q1 2018 2018.
17. Matasci, S. Solar Panel Cost: Avg. Solar Panel Prices by State in 2019: EnergySage. *Solar News, EnergySage* **2019**.
18. Dudley, D. *Renewable Energy Will Be Consistently Cheaper Than Fossil Fuels By 2020*; Forbes, 2019;
19. Solar Industry Research Data | SEIA Available online: <https://www.seia.org/solar-industry-research-data> (accessed on 2 January 2024).
20. Solar Industry Research Data Available Online.
21. Vaughan, A. Time to Shine: Solar Power Is Fastest-Growing Source of New Energy. *The Guardian* **2017**.
22. Barbose, G.L.; Darghouth, N.R.; LaCommare, K.H.; Millstein, D.; Rand, J. Tracking the Sun: Installed Price Trends for Distributed Photovoltaic Systems in the United States-2018 Edition 2018.
23. Calvert, K.; Mabee, W. More Solar Farms or More Bioenergy Crops? Mapping and Assessing Potential Land-Use Conflicts among Renewable Energy Technologies in Eastern Ontario, Canada. *Applied Geography* **2015**, *56*, 209–221, doi:10.1016/j.apgeog.2014.11.028.
24. Calvert, K.; Pearce, J.M.; Mabee, W.E. Toward Renewable Energy Geo-Information Infrastructures: Applications of GIScience and Remote Sensing That Build Institutional Capacity. *Renewable and Sustainable Energy Reviews* **2013**, *18*, 416–429, doi:10.1016/j.rser.2012.10.024.
25. Sovacool, B.K. Exploring and Contextualizing Public Opposition to Renewable Electricity in the United States. *Sustainability* **2009**, *1*, 702–721, doi:10.3390/su1030702.
26. Sovacool, B.K.; Lakshmi Ratan, P. Conceptualizing the Acceptance of Wind and Solar Electricity. *Renewable and Sustainable Energy Reviews* **2012**, *16*, 5268–5279, doi:10.1016/j.rser.2012.04.048.
27. Pearce, J.M. Agrivoltaics in Ontario Canada: Promise and Policy. *Sustainability* **2022**, *14*, 3037, doi:10.3390/su14053037.
28. Dupraz, C.; Marrou, H.; Talbot, G.; Dufour, L.; Nogier, A.; Ferard, Y. Combining Solar Photovoltaic Panels and Food Crops for Optimising Land Use: Towards New Agrivoltaic Schemes. *Renewable Energy* **2011**, *36*, 2725–2732, doi:10.1016/j.renene.2011.03.005.
29. Guerin, T.F. Impacts and Opportunities from Large-Scale Solar Photovoltaic (PV) Electricity Generation on Agricultural Production. *Environmental Quality Management* **2019**, *28*, 7–14, doi:10.1002/tqem.21629.
30. Valle, B.; Simonneau, T.; Sourd, F.; Pechier, P.; Hamard, P.; Frisson, T.; Ryckewaert, M.; Christophe, A. Increasing the Total Productivity of a Land by Combining Mobile Photovoltaic Panels and Food Crops. *Applied Energy* **2017**, *206*, 1495–1507, doi:10.1016/j.apenergy.2017.09.113.

31. Mavani, D.D.; Chauhan, P.M.; Joshi, V. Beauty of Agrivoltaic System Regarding Double Utilization of Same Piece of Land for Generation of Electricity & Food Production. **2019**, *10*.
32. Trommsdorff, M.; Kang, J.; Reise, C.; Schindele, S.; Bopp, G.; Ehmann, A.; Weselek, A.; Högy, P.; Obergfell, T. Combining Food and Energy Production: Design of an Agrivoltaic System Applied in Arable and Vegetable Farming in Germany. *Renewable and Sustainable Energy Reviews* **2021**, *140*, 110694, doi:10.1016/j.rser.2020.110694.
33. Mow, B. Solar Sheep and Voltaic Veggies: Uniting Solar Power and Agriculture Available online: <https://www.nrel.gov/state-local-tribal/blog/posts/solar-sheep-and-voltaic-veggies-uniting-solar-power-and-agriculture.html> (accessed on 1 April 2023).
34. Nassar, A.; Perez-Wulf, I.; Hameiri, Z. Improving Productivity of Cropland through Agrivoltaics.; 2020.
35. Amaducci, S.; Yin, X.; Colauzzi, M. Agrivoltaic Systems to Optimise Land Use for Electric Energy Production. *Applied Energy* **2018**, *220*, 545–561, doi:10.1016/j.apenergy.2018.03.081.
36. Reasoner, M.; Ghosh, A. Agrivoltaic Engineering and Layout Optimization Approaches in the Transition to Renewable Energy Technologies: A Review. *Challenges* **2022**, *13*, 43, doi:10.3390/challe13020043.
37. Kumpanalaisatit, M.; Setthapun, W.; Sintuya, H.; Pattiya, A.; Jansri, S.N. Current Status of Agrivoltaic Systems and Their Benefits to Energy, Food, Environment, Economy, and Society. *Sustainable Production and Consumption* **2022**, *33*, 952–963, doi:10.1016/j.spc.2022.08.013.
38. Giri, N.C.; Mohanty, R.C. Agrivoltaic System: Experimental Analysis for Enhancing Land Productivity and Revenue of Farmers. *Energy for Sustainable Development* **2022**, *70*, 54–61, doi:10.1016/j.esd.2022.07.003.
39. Food Security Structures Canada Available online: <https://www.foodsecuritystructures.ca/home> (accessed on 25 March 2024).
40. Food Security Structures Canada - Better Grow Lights Available online: <https://www.foodsecuritystructures.ca/growing-systems/better-grow-lights> (accessed on 29 February 2024).
41. Bhatia, A. Cooling Load Calculations and Principles. *Continuing Education and Development, Inc. New York* **2001**, *877*, 39.
42. Handbook, A.F. ASHRAE Fundamentals Handbook. **1997**.
43. Cengel, Y.A. Heat Transfer: A Practical Approach. (No Title) **1998**.
44. McQuiston, F.C.; Parker, J.D.; Spitler, J.D.; Taherian, H. *Heating, Ventilating, and Air Conditioning: Analysis and Design*; John Wiley & Sons, 2023; ISBN 1-119-89416-6.
45. Asgari, N.; McDonald, M.T.; Pearce, J.M. Energy Modeling and Techno-Economic Feasibility Analysis of Greenhouses for Tomato Cultivation Utilizing the Waste Heat of Cryptocurrency Miners. *Energies* **2023**, *16*, 1331, doi:10.3390/en16031331.
46. Kumar, R.; Shankar, V.; Kumar, M. Modelling of Crop Reference Evapotranspiration: A Review.
47. Subedi, A.; Chávez, J.L. Crop Evapotranspiration (ET) Estimation Models: A Review and Discussion of the Applicability and Limitations of ET Methods. *JAS* **2015**, *7*, p50, doi:10.5539/jas.v7n6p50.
48. Ultimate-Grow-Room-HVAC-Guide.Pdf.
49. <https://www.facebook.com/Profile.php?id=61551502111382&paipv=0&eav=AfYQpquxSgYutdhvY6b9vsFe2ytRVgTMf55dnauXuvJBURJMBE2cxoThPjTzaFtEKCY> Available online: <https://www.facebook.com/profile.php?id=61551502111382&paipv=0&eav=AfYQpquxSgYutdhvY6b9vsFe2ytRVgTMf55dnauXuvJBURJMBE2cxoThPjTzaFtEKCY> (accessed on 25 March 2024).
50. Heat Pump | GSZ16 | up to 16 SEER | 9.0 HSPF | Goodman Available online: <https://www.goodmanmfg.com/products/heat-pumps/16-seer-gsz16> (accessed on 25 March 2024).
51. Li, S.; Gong, G.; Peng, J. Dynamic Coupling Method between Air-Source Heat Pumps and Buildings in China's Hot-Summer/Cold-Winter Zone. *Applied Energy* **2019**, *254*, 113664, doi:10.1016/j.apenergy.2019.113664.
52. Available online: <https://web.emporiaenergy.com/> (accessed on 3 April 2024).
53. NOMA 50 Pint LED Dehumidifier with Pump, Bucket/Continuous Drain, ENERGY STAR® Most Efficient, White | Canadian Tire Available online: <https://www.canadiantire.ca/en/pdp/noma-50-pint-led-dehumidifier-with-pump-bucket-continuous-drain-energy-star-most-efficient-white-0430755p.html> (accessed on 27 March 2024).
54. Rule of Thumb Calculations (400 Cfm/Ton) Available online: https://tranecds.custhelp.com/app/answers/detail/a_id/918/~rule-of-thumb-calculations-%28400-cfm%2Fton%29 (accessed on 2 April 2024).

55. National Renewable Energy Laboratory SAM Open Source - System Advisor Model - SAM. Available online: <https://sam.nrel.gov/about-sam/sam-open-source.html> (accessed on 15 December 2022).
56. Ciocia, A.; Amato, A.; Di Leo, P.; Fichera, S.; Malgaroli, G.; Spertino, F.; Tzanova, S. Self-Consumption and Self-Sufficiency in Photovoltaic Systems: Effect of Grid Limitation and Storage Installation. *Energies* **2021**, *14*, 1591, doi:10.3390/en14061591.
57. Asgari, N.; Hayibo, K.S.; Groza, J.; Rana, S.; Pearce, J.M. Greenhouse Applications of Solar Photovoltaic Driven Heat Pumps in Northern Environments, Western University, London, ON, Canada. *Under Review* **2024**.
58. Rana, S.; Jamil, U.; Asgari, N.; Hayibo, K.S.; Groza, J.; Pearce, J.M. Residential Sizing of Solar Photovoltaic Systems and Heat Pumps for Net Zero Sustainable Thermal Building Energy. *Computation* **2024**, *12*, 126, doi:10.3390/computation12060126.
59. Heliene 144HC M6 Bifacial Module 144 Half-Cut Monocrystalline 440W – 460W (HSPE-144HC-M6-Bifacial-Rev.05.Pdf) 2022.
60. Hayibo, K.S.; Pearce, J.M. Vertical Free-Swinging Photovoltaic Racking Energy Modeling: A Novel Approach to Agrivoltaics. *Renewable Energy* **2023**, *218*, 119343, doi:10.1016/j.renene.2023.119343.
61. Solar Power Calculator Ontario, Canada Available online: <https://solarcalculator.ca/province/Ontario/> (accessed on 22 June 2024).
62. Alberta, S. Winter Effects on Solar PV Efficiency Available online: <https://solaralberta.ca/members/business-member-resources/alberta-solar-performance-data/> (accessed on 22 June 2024).
63. Robinson, A. Solar PV Analysis of Houston, United States Available online: <https://profilesolar.com/locations/United-States/Houston/> (accessed on 22 June 2024).
64. Solar Panel Installation Info - Montreal | Quebec Solar 2024.
65. Solar Panel Angles for San Francisco, California, US Available online: <https://solarific.co> (accessed on 22 June 2024).
66. London International Airport | Weather History & Climate Available online: <https://meteostat.net/en/station/71623?t=2024-02-17/2024-02-24> (accessed on 13 June 2024).
67. Castilla, N. *Greenhouse Technology and Management*; Cabi, 2013; ISBN 1-78064-103-6.
68. Sustainability | Free Full-Text | The Agrivoltaic Potential of Canada Available online: <https://www.mdpi.com/2071-1050/15/4/3228> (accessed on 24 June 2024).
69. D'Souza, S.; Guerriero, L.; Ellenwood, L.; Angelovski, I. What's behind Rising Food Costs in Canada's North? Questions Emerge over How Retailer Sets Prices. *CBC News* 2024.
70. Lessons from Vertical Farming Bankruptcies, Layoffs, and Closures in 2023 Available online: <https://www.verticalfarmdaily.com/article/9537965/lessons-from-vertical-farming-bankruptcies-layoffs-and-closures-in-2023/> (accessed on 23 June 2024).
71. Riemenschneider, P. Indoor Farming Operations Face Bankruptcies, Layoffs, Closures. *Produce Blue Book*.
72. Johnson, G. 80 Acres Farms Makes Layoffs. *Produce Blue Book*.
73. Riemenschneider, P. AppHarvest Opens 60-Acre Kentucky Farm, Completes \$127MM Sale-Leaseback with Mastronardi Barea LLC. *Produce Blue Book*.
74. Riemenschneider, P. AppHarvest Opens Salad Farm Backed by \$30 Million Mastonardi Produce Loan. *Produce Blue Book*.
75. Johnson, G. Edible Garden Approves Reverse Stock Split. *Produce Blue Book*.
76. Riemenschneider, P. Faced with Nasdaq Delisting, Kalera Shareholders Approve Reverse Stock Split. *Produce Blue Book*.
77. Riemenschneider, P. Kalera Halts Orlando, Atlanta Production to Focus on Profitability at Other Facilities. *Produce Blue Book*.
78. Heater, B. Iron Ox Lays off 50, Amounting to Nearly Half Its Staff Available online: <https://techcrunch.com/2022/11/03/iron-ox-lays-off-50-amounting-to-nearly-half-its-staff/> (accessed on 23 June 2024).
79. Marston, J. Brief: Plenty Confirms Closure of South San Francisco Vertical Farming Facility Available online: <https://agfundernews.com/plenty-confirms-closure-of-south-san-francisco-vertical-farming-facility> (accessed on 23 June 2024).
80. Johnson, G. Lakeside Produce Files Bankruptcy, Owes \$188MM. *Produce Blue Book*.

81. Vertical Farming Robotics Startup Fifth Season Shuts Down Available online: <https://www.bizjournals.com/pittsburgh/news/2022/10/29/vertical-farming-startup-fifth-season-shuts-down.html> (accessed on 23 June 2024).
82. Indoor Agriculture Faces a Reckoning | Ambrook Research Available online: <https://ambrook.com/research/supply-chain/vertical-farms-venture-capital-chapter-11> (accessed on 23 June 2024).
83. Indoor Farming Company AppHarvest Files for Bankruptcy Available online: <https://www.agriculturediver.com/news/appharvest-bankruptcy-indoor-farming-martha-stewart-jd-vance/689039/> (accessed on 23 June 2024).
84. As Indoor Farming Startups with Hundreds of Millions in Funding Head to Bankruptcy, Critic Says: “Boy, This Is a Dumb Idea” Available online: <https://fortune.com/2023/09/18/indoor-farming-startups-bankruptcy-dumb-idea-expensive/> (accessed on 23 June 2024).

Disclaimer/Publisher’s Note: The statements, opinions and data contained in all publications are solely those of the individual author(s) and contributor(s) and not of MDPI and/or the editor(s). MDPI and/or the editor(s) disclaim responsibility for any injury to people or property resulting from any ideas, methods, instructions or products referred to in the content.